

A genetically encoded fluorescent acetylcholine indicator for *in vitro* and *in vivo* studies

Miao Jing^{1–3,16}, Peng Zhang^{4,16}, Guangfu Wang^{4,5}, Jiesi Feng^{1–3}, Lukas Mesik⁶, Jianzhi Zeng^{1–3}, Huoqing Jiang^{1–3}, Shaohua Wang⁷, Jess C Looby^{4,8}, Nick A Guagliardo⁴, Linda W Langma⁹, Ju Lu¹⁰, Yi Zuo¹⁰, David A Talmage⁷, Lorna W Role⁷, Paula Q Barrett⁴, Li I Zhang⁶, Minmin Luo^{11,12}, Yan Song³, J Julius Zhu^{4,13–15} & Yulong Li^{1–3}

The neurotransmitter acetylcholine (ACh) regulates a diverse array of physiological processes throughout the body. Despite its importance, cholinergic transmission in the majority of tissues and organs remains poorly understood owing primarily to the limitations of available ACh-monitoring techniques. We developed a family of ACh sensors (GACH) based on G-protein-coupled receptors that has the sensitivity, specificity, signal-to-noise ratio, kinetics and photostability suitable for monitoring ACh signals *in vitro* and *in vivo*. GACH sensors were validated with transfection, viral and/or transgenic expression in a dozen types of neuronal and non-neuronal cells prepared from multiple animal species. In all preparations, GACH sensors selectively responded to exogenous and/or endogenous ACh with robust fluorescence signals that were captured by epifluorescence, confocal, and/or two-photon microscopy. Moreover, analysis of endogenous ACh release revealed firing-pattern-dependent release and restricted volume transmission, resolving two long-standing questions about central cholinergic transmission. Thus, GACH sensors provide a user-friendly, broadly applicable tool for monitoring cholinergic transmission underlying diverse biological processes.

Acetylcholine (ACh), the first identified neurotransmitter, mediates cell-to-cell communication in the central and peripheral nervous systems, as well as non-neuronal systems^{1–7}. Cholinergic projection neurons within the mammalian brain originate primarily in three major nuclei, including the basal forebrain, the brainstem pedunculopontine, and laterodorsal tegmental nuclei in the brainstem. Cholinergic neurons within these groups project widely throughout the cortical and subcortical domains, consistent with their involvement in complex brain functions, including attention, perception, associative learning, and sleep/awake balancing^{1–5}. Additional smaller populations of cholinergic neurons scatter throughout other brain areas (e.g., the medial habenula (MHb) and the striatum), contributing to behaviors related to motion, motivation, and stress^{1,3,8}. Dysregulation of central cholinergic transmission is linked to a number of brain disorders, including Alzheimer's disease, addiction, epilepsy, Parkinson's disease, schizophrenia, and depression^{9,10}. In the peripheral nervous and non-nervous systems, ACh is released by both neurons and non-neuronal cells to relay fast transmission at neuromuscular junctions and to regulate functions of a variety of other tissues and organs, including the heart, liver, and pancreas^{5–7}. Dysregulation of peripheral and non-neuronal cholinergic signals is associated with multiple pathological

states, including cardiovascular disease, diabetes, immune deficiency, and cancer^{11,12}.

Despite the significance of ACh signals in many fundamental aspects of our physiology, cholinergic transmission in the majority of tissues and organs remains poorly understood, due primarily to the limitations of tools available for the direct measurement of ACh^{1,5,13}. Microdialysis, an established method for monitoring extracellular ACh¹⁴, is less frequently used because of its poor spatial and temporal resolution. Patch-clamp recordings have excellent sensitivity and temporal resolution, but the approach is limited by the number of cells that can be recorded simultaneously and the prominent desensitization of cholinergic currents³. Similarly, ACh amperometry has millisecond temporal resolution, yet its technically challenging enzymatic coating procedure limits its stability and reproducibility¹⁵. While the TANGO assay has unparalleled sensitivity, the time-consuming transcriptional and translational amplification processes prevent its use for real-time ACh measurements¹⁶. Recently developed FRET sensors and cell-based fluorescent sensors (CNiFERS) for ACh have attractive real-time imaging features, but they are limited by either the low sensitivity^{17,18} or the dependence on invasive cell transplantation^{19,20}. These fluorescent

¹State Key Laboratory of Membrane Biology, Peking University School of Life Sciences, Beijing, China. ²PKU-IDG/McGovern Institute for Brain Research, Beijing, China. ³Peking-Tsinghua Center for Life Sciences, Beijing, China. ⁴Department of Pharmacology, University of Virginia School of Medicine, Charlottesville, Virginia, USA. ⁵Center for Life Sciences, School of Life Science and Technology, Harbin Institute of Technology, Harbin, China. ⁶Zilkha Neurogenetic Institute, Department of Physiology & Neuroscience, Keck School of Medicine, University of Southern California, Los Angeles, California, USA. ⁷Department of Neurobiology and Behavior, Stony Brook University, Stony Brook, New York, USA. ⁸Undergraduate Class of 2019, University of Virginia College of Arts and Sciences, Charlottesville, Virginia, USA. ⁹Department of Surgery, University of Virginia School of Medicine, Charlottesville, Virginia, USA. ¹⁰Department of Molecular, Cell, and Developmental Biology, University of California, Santa Cruz, California, USA. ¹¹School of Life Sciences, Tsinghua University, Beijing, China. ¹²National Institute of Biological Sciences, Beijing, China. ¹³School of Medicine, Ningbo University, Ningbo, China. ¹⁴Donders Institute for Brain, Cognition and Behavior, Radboud University Nijmegen, Nijmegen, the Netherlands. ¹⁵Department of Physiology, School of Basic Medicine, Tongji Medical College, Huazhong University of Science and Technology, Wuhan, China. ¹⁶These authors contributed equally to this work. Correspondence should be addressed to J.J.Z. (jjzhu@virginia.edu) or Y.L. (yulongli@pku.edu.cn).

Received 5 May 2017; accepted 30 April 2018; published online 9 July 2018; doi:10.1038/nbt.4184

sensors, nevertheless, inspired us to engineer more user-friendly and broadly applicable genetically encoded ACh sensors^{19,21}.

Here, we report a family of genetically encoded G-protein-coupled receptor activation-based sensors for ACh (GACH). Our GACH sensors were initially constructed by coupling a circular permuted green fluorescent protein (cpGFP) into a muscarinic acetylcholine receptor (MR), with subsequent improvements via large-scale, site-directed mutagenesis and screening. The sensitivity and utility of GACH sensors were validated in cultured HEK293T cells, in cultured cortical neurons, in tissue slices prepared from multiple brain regions and peripheral organs, in the olfactory system of living *Drosophila*, and in the visual cortex of freely behaving mice *in vivo*. Our data indicate that GACH sensors have the sensitivity ($EC_{50} \approx 1 \mu M$), specificity (comparable to endogenous MRs), signal-to-noise ratio (SNR ≈ 14), kinetics ($\tau_{on/off} \approx 200-800 \text{ ms}$) and photostability ($\geq 1-4 \text{ h}$) suitable for precise and convenient real-time assays of ACh signals.

RESULTS

Development and optimization of GACH sensors

We first inserted a conformationally sensitive cpGFP into the third intracellular loop (ICL₃) of five subtypes of human muscarinic acetylcholine receptors (M₁₋₅Rs) (Fig. 1a and Supplementary Fig. 1). ICL₃ was chosen because it links the transmembrane helices 5 and 6 of MRs and may undergo a large conformational change upon ACh binding²². We replaced ICL₃ of M₁₋₅Rs with a shorter 54-amino acid ICL₃ modified from the structurally well-characterized β_2 adrenergic receptor (β_2 AR)²³ to avoid creating a lengthy cpGFP-containing ICL₃ that may hinder the expression and trafficking of the proteins (Supplementary Fig. 1a). Cells expressing the M₃R chimera showed excellent membrane expression in HEK293T cells and increased fluorescence responses ($\Delta F/F_0$) (by $\sim 30\%$) to bath application of ACh (Fig. 1b and Supplementary Fig. 1a). In contrast, cells expressing the other four MR chimeras all exhibited poor membrane expression and no detectable $\Delta F/F_0$ upon ACh application (Supplementary Fig. 1b-d).

To improve this new ACh sensor (named GACH1.0), we used site-directed mutagenesis to create a library of 723 randomized point mutations at the N terminus two-amino acid and C terminus five-amino acid linkers that connect cpGFP and M₃R (Fig. 1c and Supplementary Fig. 2). When expressed in HEK293T cells, we found variants with one or multiple single-point mutations on the seven linker residues (total 18 hits) produced relatively larger $\Delta F/F_0$ responses, with the best variant (named GACH1.5) producing a $\sim 70\%$ increase in $\Delta F/F_0$ (Fig. 1c,d and Supplementary Fig. 2). In a second round of site-directed mutagenesis and screening, we used combinations of single top hits on N terminus linker residues (i.e., GG) and two to four top hits on C terminus linker residues, and found one variant (named GACH2.0) out of 23 combinatorial variants with the best $\Delta F/F_0$ (Fig. 1c and Supplementary Fig. 2). GACH2.0 had the same expression and membrane trafficking properties and enhanced dynamic range (by 2.5-fold) compared to GACH1.0 (Fig. 1e-g and Supplementary Movie 1), and ~ 20 -fold larger peak signal responses and ~ 60 -fold higher signal-to-noise ratio (SNR) compared to M₁R-based FRET sensor¹⁸ (Fig. 1h-j and Supplementary Fig. 3).

Characterization of GACH sensors in cultured cells

Next, we measured the response kinetics of GACH2.0 (Fig. 2a,b). High-speed imaging showed that rapid local perfusion of agonist ACh or antagonist tiotropium (Tio) elicited increases or decreases in fluorescence intensity of GACH2.0, with average activation (on) and inactivation (off) time constants of $280 \pm 32 \text{ ms}$ and $762 \pm 75 \text{ ms}$,

respectively (Fig. 2b,c). These values were likely overestimated due to the slow drug application/perfusion system ($\sim 80 \text{ ms}$ delay, Supplementary Fig. 4). Moreover, confocal imaging indicated that GACH sensors had a photostability comparable to or better than GCaMP6s and EGFP (Supplementary Fig. 5). Altering extracellular pH with buffers (pH 5–9) resulted in modest fluorescence changes in GACH-expressing cells (Supplementary Fig. 6a,b), suggesting a weak pH dependency. In the permeabilized condition, the fluorescence of GACH sensors exhibited larger pH dependency with a pK_a close to 7 (Supplementary Fig. 6c,d).

To measure the sensitivity of GACH2.0, we progressively increased ACh from 10 nM to 100 μM , which increased the fluorescence intensity in GACH2.0-expressing cells, yielding an EC_{50} (concentration for 50% maximal effect) of $\sim 0.7 \mu M$ (Fig. 2d,e), a value comparable to wild-type M₃Rs²⁴. ACh-induced fluorescence signals were completely blocked by co-application of 20 μM AF-DX 384, another muscarinic antagonist²⁵, indicating specific responses. We also characterized the downstream signaling of GACH sensors. GACH2.0-expressing cells exhibited less receptor internalization in the presence of ACh, as well as reduced TANGO assay signal (β -arrestin-dependent) compared to wild-type M₃Rs-expressing cells (Supplementary Fig. 7a,b). Moreover, the coupling efficiency from GACH2.0 to the Gq-dependent calcium signaling was about sevenfold smaller compared to wild-type M₃Rs (Supplementary Fig. 7c-e), and there was no detectable coupling of GACH2.0 to the Gs-dependent signaling pathway (Supplementary Fig. 7f-h).

We next verified several properties of GACH sensors in cultured rat cortical neurons (Fig. 2f-j). Approximately 48 h after transfection, GACH1.0 and GACH2.0 were expressed throughout the neuronal membrane, with the majority of sensors delivered to the neurites (Fig. 2f). ACh enhanced the fluorescence intensity of GACH1.0 and GACH2.0 by $\sim 30\%$ and $\sim 90\%$, respectively (Fig. 2g and Supplementary Movie 2), validating their functionality in neurons. Varying ACh concentration in the bath solution from 10 nM to 100 μM progressively increased the fluorescence intensity in GACH2.0-expressing neurons, with an EC_{50} of $\sim 2 \mu M$ (Fig. 2h). In contrast, bath application of nicotine, choline, glycine, serotonin (5-HT), epinephrine, GABA, glutamate, dopamine, norepinephrine, histamine, and adenosine did not induce any detectable fluorescence responses. Moreover, ACh-induced fluorescence responses were blocked by bath-applied Tio (Fig. 2i,j). Finally, we noted no alteration in membrane fluorescence intensity in GACH2.0-expressing neurons during a 30-min bath application of 100 μM ACh (Supplementary Fig. 8a-c), consistent with the minimal arrestin-dependent internalization (Supplementary Fig. 7a,b).

Validation of GACH sensors in cultured brain slices

To generalize the applicability of GACH sensors, we expressed them in CA1 pyramidal neurons in cultured mouse hippocampal slices. Two-photon imaging showed that GACH1.0, GACH1.5, and GACH2.0 were expressed throughout CA1 pyramidal neurons by the lentiviral system, with evident fluorescence signals at the plasma membrane of somata, dendrites, and spines, sites of excitatory synapses (Supplementary Fig. 9). Next, we chose the Sindbis viral expression system that permitted a more rapid ($\sim 18 \text{ h}$) and robust expression of GACH sensors (Supplementary Figs. 10a and 11a). Fluorescence responses captured by an epifluorescence microscope showed that a brief 500-ms puff application of ACh or the muscarinic agonist oxotremorine²⁴ evoked fluorescence responses in CA1 neurons expressing GACH1.0, GACH1.5, or GACH2.0, whereas puff application of a nicotinic receptor agonist, nicotine, or control bath solution ACSF induced no responses in same neurons (Supplementary Figs. 10b-d and 11b and Supplementary Movies 3 and 4).

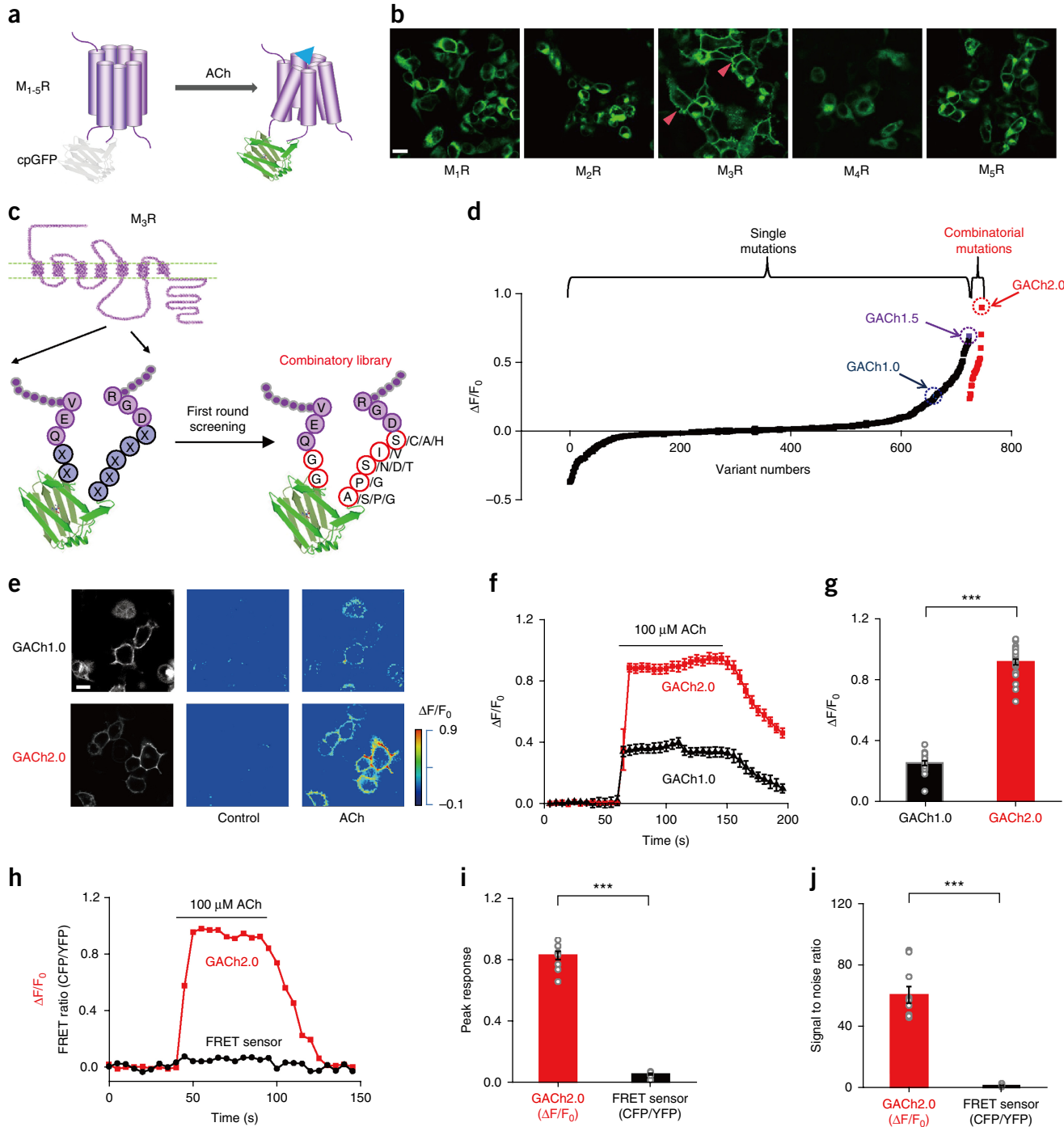
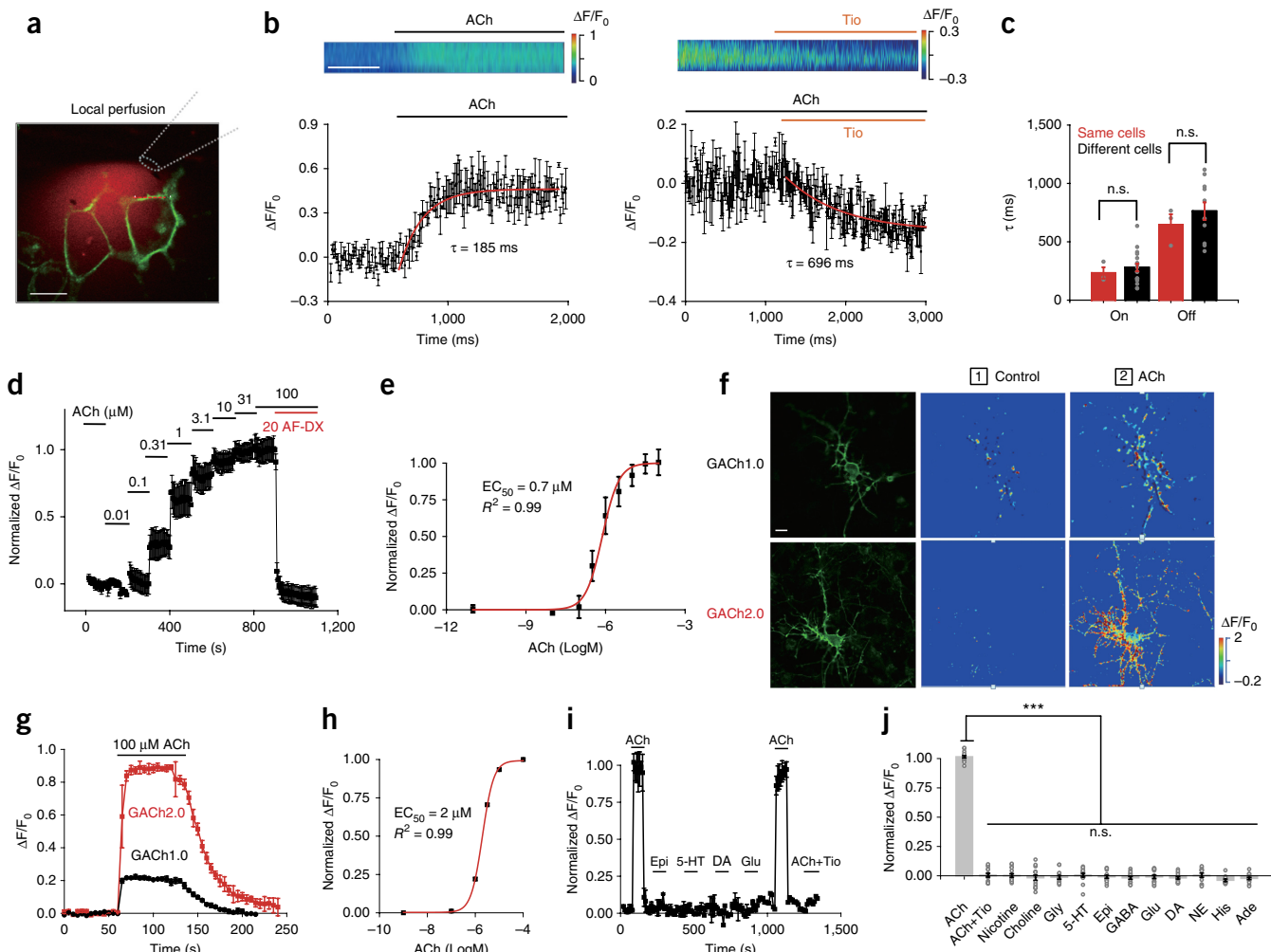


Figure 1 Development of GACH sensors. **(a)** Schematic drawing shows the principle of the GACH sensor. **(b)** Membrane expression of the different MR-based candidate GACH sensors in HEK293T cells. The red arrow heads indicate membrane-localized signals. **(c)** Schematic drawing illustrates variants with one or multiple single-point mutations on the seven linker residues (total 18 hits). **(d)** Fluorescence responses of HEK293T cells expressing one of ~750 candidate GACH sensors harboring either randomized point or combinatorial mutations to the bath application of 100 μ M ACh. Note $\Delta F/F_0$ of the combinatorial mutation-harboring GACH2.0 to be ~100% and data points are averaged responses of 2–10 cells. **(e)** Fluorescence responses of GACH1.0- and GACH2.0-expressing cells to the bath application of ACh. **(f,g)** $\Delta F/F_0$ of GACH1.0- and GACH2.0-expressing cells to ACh application (GACH1.0: $24.6 \pm 1.5\%$, $n = 19$ cells from five cultures, GACH2.0: $90.1 \pm 1.7\%$, $n = 29$ cells from eight cultures, $U = 551$, $P = 6.72 \times 10^{-9}$). **(h)** Fluorescence responses of HEK293T cells expressing either GACH2.0 or M₁R-based FRET sensor to the application of ACh (100 μ M). **(i,j)** Averaged $\Delta F/F_0$ or $\Delta FRET$ ratio (GACH2.0: $94.0 \pm 3.0\%$, $n = 10$ cells from two cultures; FRET: $6.61 \pm 0.4\%$, $n = 10$ cells from two cultures, $U = 100$, $P = 1.09 \times 10^{-5}$) and SNR (GACH2.0: 60.0 ± 5.4 , $n = 10$ cells from two cultures; FRET: 1.12 ± 0.21 , $n = 10$ cells from two cultures, $U = 100$, $P = 1.83 \times 10^{-4}$) of GACH2.0 and M₁R-based FRET-sensor-expressing cells to ACh application. Data are shown as mean \pm s.e.m., with error bars indicating s.e.m. Experiments in **b** and **e** were repeated independently for more than five cultures with similar results. *** $P < 0.001$ (Mann–Whitney Rank Sum non-parametric tests, two-sided). All scale bars, 10 μ m.

Focusing on GACH2.0, which produces the largest $\Delta F/F_0$, we found that repetitive puffs induced the same fluorescence responses in GACH2.0-expressing CA1 neurons (Supplementary Fig. 12),

indicating robust photostability. As a control, bath application of 1 μM atropine, a muscarinic antagonist²⁵, but not 2,2,6,6-tetramethylpiperidin-4-yl heptanoate (TMPh), a nicotinic antagonist²⁶, completely



blocked ACh-induced fluorescence responses in GACh2.0-expressing neurons (**Supplementary Fig. 12**). Simultaneous patch-clamp recordings showed that the resting membrane potential, input resistance, membrane time constant and average spiking frequency of GACh2.0-expressing CA1 neurons were not different from nearby control non-expressing neurons (**Supplementary Fig. 13a–d**), suggesting GACh2.0 expression had no effect on basic membrane properties. Moreover, AMPA, NMDA, and GABAergic responses, as well as paired pulse facilitation of AMPA responses in GACh2.0-expressing neurons, remained unchanged (**Supplementary Fig. 13e–h**), indicating GACh2.0 expression did not alter synaptic transmission. Collectively, these results are consistent with the finding that GACh2.0 is a selective, photostable ACh sensor with minimal perturbation on cellular physiology.

To compare GACh2.0 imaging with patch-clamp recordings, we simultaneously made whole-cell recordings and fluorescence imaging from pairs of neighboring GACh2.0-expressing and non-expressing CA3 pyramidal neurons, which performed robust current response to cholinergic stimulation in cultured mouse hippocampal slices²⁷ (**Fig. 3a**). A 500-ms ACh puff evoked a brief, large inward current followed by a prolonged, small inward current in both GACh2.0-expressing and non-expressing neurons, presumably representing activation of endogenous nicotinic and muscarinic receptors, respectively³ (**Fig. 3b,d**). A concurrent fluorescence signal was observed only in GACh2.0-expressing neurons, but not in control non-expressing CA3 neurons (**Fig. 3b,c**). The latencies of cholinergic currents and fluorescence responses were the same in GACh2.0-expressing neurons (**Fig. 3b,e**), indicating that GACh2.0 detected ACh as fast as endogenous cholinergic receptors. SNR of GACh2.0 fluorescence responses (~14) seemed to be smaller than that of the fast nicotinic-like cholinergic currents (~35), but larger than that of the slow muscarinic-like cholinergic currents (~8) (**Fig. 3b,f**), indicating a relatively comparable sensitivity for GACh2.0 to electrophysiological recording in monitoring cholinergic signals. The second ACh puff evoked same fluorescence responses, but smaller cholinergic currents (reduced by ~40%) in GACh2.0-expressing neurons compared to the first ACh puff (**Fig. 3b,g,h**), due presumably to the desensitization of endogenous receptors³. There was no difference in the amplitude, latency, or SNR of cholinergic currents in GACh2.0-expressing and non-expressing neurons (**Fig. 3b–f**), further confirming that expression of GACh2.0 had little non-specific effect on CA3 neurons.

GACh sensors in acute brain slices

We next imaged the fluorescence response of GACh2.0 in acute slices of distinct neuronal preparations, including layer 2 (L2) stellate neurons and L1 interneurons in the medial entorhinal cortex (MEC), L5 pyramidal neurons in the barrel cortex of mice, GABAergic thalamic reticular neurons, and glutamatergic thalamocortical neurons in the ventral basal nucleus of rats. Approximately 18 h after *in vivo* Sindbis viral expression and acute slice preparation, we measured $\Delta F/F_0$ responses to a brief puff application of ACh (**Supplementary Fig. 14a**). ACh and oxotremorine, but not nicotine or control bath solution ACSF, evoked robust fluorescence increases in GACh2.0-expressing neurons in all the preparations (**Supplementary Fig. 14**).

To further test whether GACh2.0 can report endogenously released ACh, we measured $\Delta F/F_0$ responses of GACh2.0-expressing entorhinal L2 stellate neurons to electrical stimulation of MEC L1 (**Fig. 4a**), a layer that is densely innervated by cholinergic fibers originating from the basal forebrain^{28,29}. In GACh2.0-expressing neurons, 20 pulses at 2-Hz evoked robust fluorescence responses in GACh2.0-expressing

neurons (**Fig. 4b** and **Supplementary Movie 5**), and repeated electrical stimuli delivered every 8 min induced the same $\Delta F/F_0$ responses in GACh2.0-expressing neurons (**Fig. 4c,d**), indicating the suitability of GACh2.0 in monitoring ACh signals over long periods. Systematically varying the stimulation frequency revealed that low-frequency stimuli (0.5–2 Hz) evoked large, plateau-like fluorescence responses, intermediate-frequency stimuli (4–12 Hz) elicited more rapidly rising but briefer fluorescence responses, while high-frequency stimuli (≥ 32 Hz) induced minor fluorescence responses (**Fig. 4e–g**). Given that basal forebrain cholinergic neurons in behaving animals prefer low frequency (~0.5–2 Hz) tonic firing and theta rhythmic (~4–12 Hz) phasic firing^{30,31}, these results suggest that these two preferred firing patterns generate distinct sustained or transient ACh release. Further altering the number of electrical pulses delivered at 2 Hz showed that single pulses elicited detectable $\Delta F/F_0$ responses, whereas multiple pulses induced enhanced $\Delta F/F_0$ responses (**Fig. 4h–j**), suggesting the possible scaling of amount of released ACh by the number of presynaptic action potentials. Of note, adding 20 μ M (5*R*,6*R*-6-(3-propylthio-1,2,5-thiadiazol-4-yl)-1-azabicyclooctane (PTAC), an antagonist of M_{1,3,5}Rs³², to the bath solution blocked the electrically evoked $\Delta F/F_0$ responses (**Supplementary Fig. 15**), indicating the detection of cholinergic signals.

We noted that at times, the minimal electrical-stimulation-evoked fluorescence responses exhibited obvious spatial heterogeneity across subcellular regions of GACh2.0-expressing L2 stellate neurons. Analysis of the evoked fluorescence responses revealed one or a few subcellular hot spots, or regions of interest (ROIs), with the largest $\Delta F/F_0$ responses, whereas other ROIs had smaller or undetectable changes in $\Delta F/F_0$ (**Fig. 4l–n**), suggesting the spatially restricted release and clearance of ACh. Plotting $\Delta F/F_0$ responses at all ROIs against the distance from the ROI with the largest $\Delta F/F_0$ responses yielded a volume transmission spread-length constant of 9.0 μ m for MEC L2 stellate neurons (**Fig. 4n**). To verify this surprisingly small cholinergic volume transmission, we examined the minimal electrical-stimulation-evoked local fluorescence responses along the somatodendritic axis of GACh2.0-expressing hippocampal CA1 neurons (**Supplementary Fig. 16a**). Consistent with previous studies²⁷, we found that electrical stimuli of the stratum-oriens and pyramidale were most likely to elicit cholinergic responses in CA1 neurons (**Supplementary Fig. 16b,c**). The largest fluorescence responses were typically observed at one or a few subcellular ROIs in the soma of GACh2.0-expressing neurons, whereas fluorescence responses at other ROIs in the soma and dendrite of the same neurons were much smaller or undetectable (**Supplementary Fig. 16b,c**). Similar analysis gave a volume transmission spread-length constant of 15.6 μ m for CA1 neurons (**Supplementary Fig. 16d**). Bath application of ACh, as a control, induced similar $\Delta F/F_0$ responses along the somatodendritic axis of GACh2.0-expressing CA1 neurons (**Supplementary Fig. 16e**), ruling out the non-specific effect of unequal expression.

To determine whether GACh sensors may report other ACh release modes, we studied neurons in the medial habenula (MHb), which potentially release ACh during high-frequency firing^{8,33}. GACh2.0 sensors were successfully expressed in interpeduncular nucleus (IPN) by adeno-associated virus (AAV), and in close proximity with MHb cholinergic fibers, verified by post hoc ChAT immunostaining (**Supplementary Fig. 17a–c**). Two-photon imaging of GACh2.0-expressing neurons showed that brief 1-, 10-, 20-, or 50-Hz 5-s electrical stimuli evoked no detectable fluorescence changes, whereas 100-Hz stimuli elicited small $\Delta F/F_0$ responses (**Supplementary Fig. 17e,g**). Bath application of GABA or GABA_B receptor agonist baclofen enhanced $\Delta F/F_0$ responses in a frequency-dependent manner, consistent with our

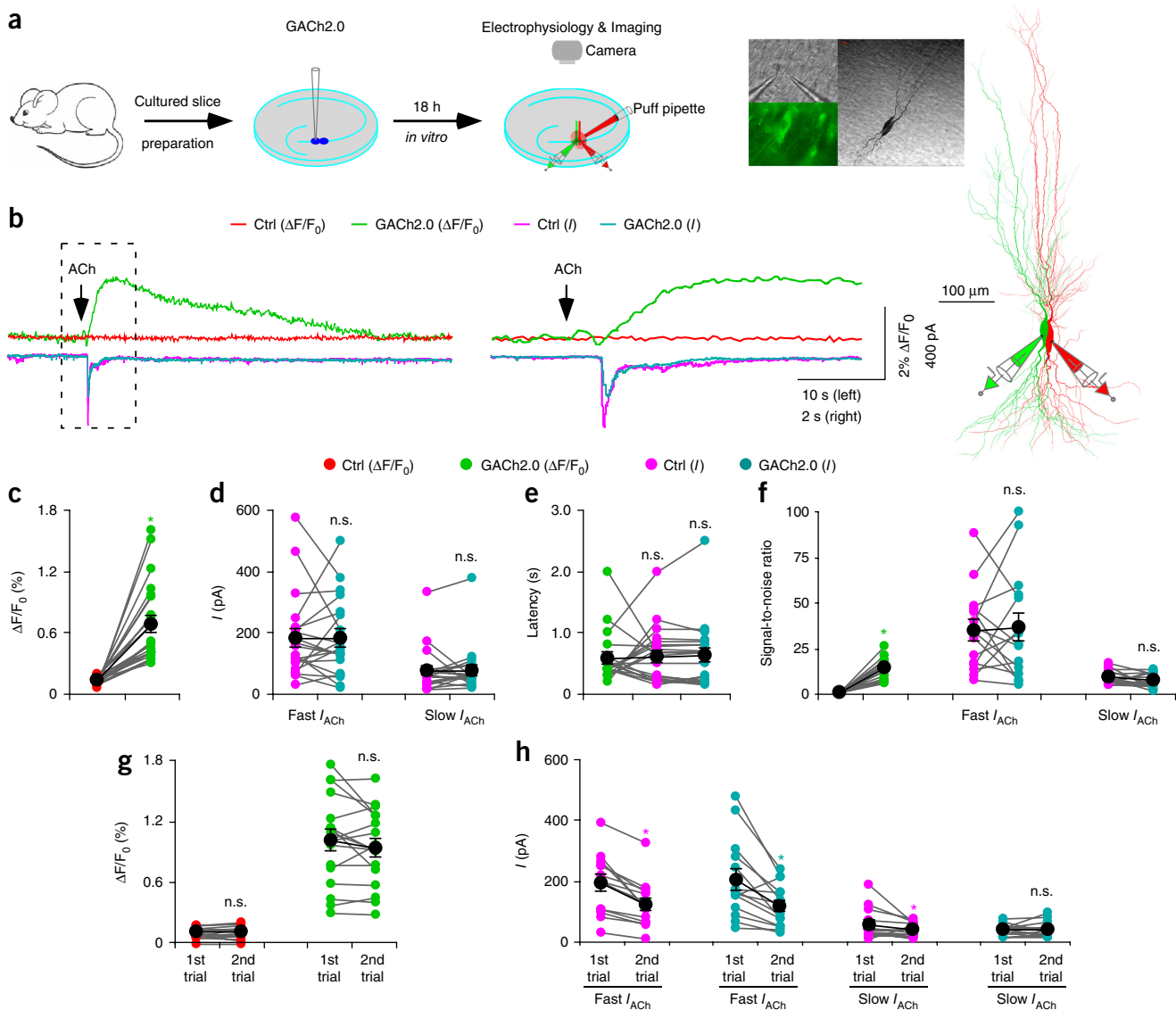


Figure 3 GACH2.0 detects rapid ACh application in brain slices. **(a)** Schematic drawing of the design of simultaneous imaging and electrophysiological recording experiments in mouse cultured hippocampal slice preparation. Left insets show transmitted light (top), fluorescence microscopic (bottom) images of a pair of simultaneously recorded GACH2.0-expressing and neighboring control non-expressing CA3 neurons. Right insets show the biocytin-filled and reconstructed GACH2.0-expressing and non-expressing CA3 neurons. **(b)** Left, simultaneous fluorescence and current responses of the pair of GACH2.0-expressing and neighboring control non-expressing CA3 neurons to a brief puff (500 ms) application of 100 mM acetylcholine (ACh). Right, the responses in the left rectangle box are shown again on an expanded time scale. **(c)** Values for the cholinergic fluorescence responses of GACH2.0-expressing CA3 neurons compared to non-expressing neurons (GACH2.0: $0.68 \pm 0.08\%$; Ctrl: $0.14 \pm 0.01\%$; $Z = 4.015$; $P = 0.0005$; $n = 21$ neurons from nine animals). **(d)** Values for the amplitudes of fast cholinergic current responses (GACH2.0: 180.9 ± 30.8 pA; Ctrl: 181.2 ± 28.4 pA; $Z = -0.037$; $P = 0.97$; $n = 21$ from nine animals) and slow cholinergic current responses (GACH2.0: 76.2 ± 15.9 pA; Ctrl: 76.8 ± 17.0 pA; $Z = 0.896$; $P = 0.37$; $n = 21$ neurons from nine animals) in GACH2.0-expressing CA3 neurons compared to non-expressing neurons. **(e)** Values for the latencies of cholinergic current responses in non-expressing CA3 neurons (Ctrl: 611 ± 10 ms; $Z = 0.523$; $P = 0.60$) and GACH2.0-expressing (GACH2.0: 622 ± 12 ms; $Z = 0.485$; $P = 0.62$) compared to those of fluorescence responses of GACH2.0-expressing neurons (GACH2.0: 580 ± 9 ms; $n = 21$ neurons from nine animals). **(f)** Values for the signal-to-noise ratio of cholinergic fluorescence responses of GACH2.0-expressing compared to non-expressing CA3 neurons (GACH2.0: 14.0 ± 1.5 ; Ctrl: 1.0 ± 0.1 ; $Z = 3.408$; $P = 0.001$; $n = 15$ neurons from six animals), and that of fast (GACH2.0: 36.2 ± 7.7 ; Ctrl: 34.6 ± 5.7 ; $Z = 0.170$; $P = 0.86$; $n = 15$ neurons from six animals) and slow (GACH2.0: 7.5 ± 1.0 ; Ctrl: 9.0 ± 1.0 ; $Z = -0.852$; $P = 0.39$; $n = 15$ neurons from six animals) cholinergic current responses of GACH2.0-expressing compared to non-expressing CA3 neurons. Note that SNR of cholinergic fluorescence responses of GACH2.0-expressing CA3 neurons is smaller than fast (GACH2.0: $Z = 2.242$; $P = 0.015$; Ctrl: $Z = 3.124$; $P = 0.002$), but larger than slow (GACH2.0: $Z = -2.840$; $P = 0.005$; Ctrl: $Z = -2.669$; $P = 0.008$) cholinergic current responses of GACH2.0-expressing compared to non-expressing CA3 neurons. **(g)** Values for the two fluorescence responses of non-expressing (1st: $0.11 \pm 0.01\%$; 2nd: $0.11 \pm 0.01\%$; $Z = -0.142$; $P = 0.89$; $n = 17$ neurons from nine animals) and GACH2.0-expressing (1st: $1.01 \pm 0.11\%$; 2nd: $0.94 \pm 0.09\%$; $Z = -1.138$; $P = 0.26$; $n = 17$ neurons from nine animals) CA3 neurons. **(h)** Values for the two fast cholinergic current responses in non-expressing (1st: 190.9 ± 26.1 pA; 2nd: 124.1 ± 20.4 pA; $Z = -3.296$; $P = 0.001$; $n = 17$ neurons from nine animals) and GACH2.0-expressing (1st: 203.8 ± 34.9 pA; 2nd: 119.3 ± 18.6 pA; $Z = -2.856$; $P = 0.004$; $n = 17$ neurons from nine animals) CA3 neurons, and values for the two slow cholinergic current responses of non-expressing (1st: 56.4 ± 13.4 pA; 2nd: 39.0 ± 5.7 pA; $Z = -2.166$; $P = 0.003$; $n = 17$ neurons from nine animals) and GACH2.0-expressing (1st: 41.6 ± 4.5 pA; 2nd: 41.7 ± 6.8 pA; $Z = 0.940$; $P = 0.93$; $n = 17$ neurons from nine animals) CA3 neurons. Data are shown as mean \pm s.e.m., where large black dots indicate mean response, error bars indicate s.e.m. * $P < 0.05$ (Wilcoxon tests, two-sided).

previous finding³³. In contrast, saclofen, a GABA_B receptor antagonist, reversed the potentiation effect. Moreover, Tio application completely abolished the ΔF/F₀ responses, while donepezil, an acetylcholinesterase inhibitor³⁴, prolonged the potentiated ΔF/F₀ responses (**Supplementary Fig. 17d,f,h–k**). These findings support the notion that extracellular GABA in IPN can drive habenula neuron firing in the physiological frequency range (up to 10–25 Hz³⁵) to release ACh, which may be critical for fear control³³.

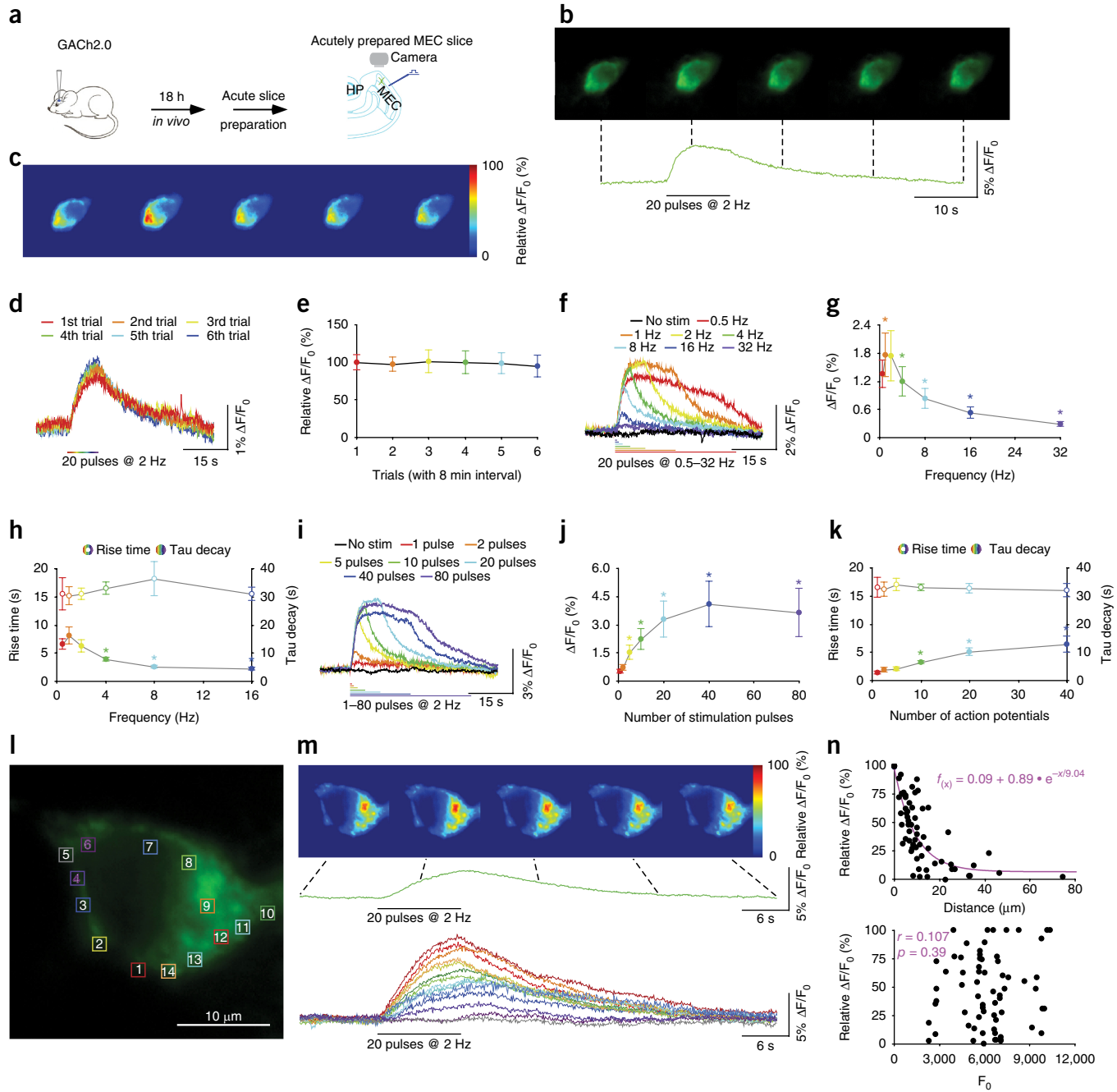
To rule out any non-specific effects that might be caused by long-term *in vivo* expression, we made chronic AAV expression of GACh2.0 in the dentate gyrus of hippocampus and examined the high K⁺-evoked calcium responses with Cal590. High K⁺ elicited the same Cal590 fluorescence responses, compared to control non-expressing neurons (**Supplementary Fig. 18**), suggesting no non-specific effect from chronic GACh2.0 expression. Moreover, we made acute cortical slices after chronic *in vivo* lentiviral expression of GACh2.0 in barrel cortical L5 pyramidal neurons in mice. Simultaneous patch-clamp recordings showed that GACh2.0-expressing and control non-expressing L5 pyramidal neurons displayed the same resting membrane potential, input resistance, membrane time constant, and average spiking frequency, as well as AMPA, NMDA, and GABAergic responses, and paired pulse facilitation of AMPA responses (**Supplementary Fig. 19**).

Figure 4 GACh2.0 reveals firing pattern-dependent restricted volume transmission in MEC. **(a)** Schematic drawing outlines the design of stimulation-imaging experiments in mouse MEC preparation. **(b)** Snapshots of fluorescence responses of the GACh2.0-expressing stellate cell to local electrical stimuli. **(c)** Relative fluorescence responses of the GACh2.0-expressing stellate cell to local electrical stimuli shown in a heat map format. **(d)** Fluorescence responses of a GACh2.0-expressing MEC stellate neuron to repetitive electrical stimulations of layer 1 every 8 min. **(e)** Values for the subsequent fluorescence responses of GACh2.0 MEC stellate neurons to multiple electrical stimulations of layer 1 at time interval of 8 min (2nd: 1.58 ± 0.15%, Z = -0.534; P = 0.59; 3rd: 1.65 ± 0.25%, Z = -0.178; P = 0.86; 4th: 1.62 ± 0.25%, Z = 0.222; P = 0.82; 5th: 1.61 ± 0.22%, Z = 0.051; P = 0.96; 6th: 1.55 ± 0.23%, Z = -0.800; P = 0.42; n = 11 neurons from seven animals) compared to the first fluorescence response (1st: 1.63 ± 0.16%). **(f)** Fluorescence responses of a GACh2.0-expressing MEC stellate neuron to electrical stimuli consisting of a train of 20 pulses at varied frequency. **(g)** Values for the peak fluorescence responses of GACh2.0-expressing MEC stellate neurons to electrical stimulations consisting of a train of 20 pulses at higher frequency (1 Hz: 1.75 ± 0.47%, Z = 2.606; P = 0.009; 2 Hz: 1.74 ± 0.53%, Z = 1.726; P = 0.08; 4 Hz: 1.19 ± 0.44%, Z = -1.746; P = 0.140; 8 Hz: 0.82 ± 0.22%, Z = -3.107; P = 0.002; 16 Hz: 0.53 ± 0.12%, Z = -3.296; P = 0.001; 32 Hz: 0.29 ± 0.06%, Z = -3.296; P = 0.001; n = 14 neurons from nine animals) compared to the lowest frequency tested (0.5 Hz: 1.34 ± 0.30%). **(h)** Values for 10–90% rise time of the fluorescence responses of GACh2.0-expressing MEC stellate neurons to electrical stimulations consisting of a train of 20 pulses at higher frequency (1 Hz: 8.1 ± 1.5 s, Z = 1.859; P = 0.06; 2 Hz: 6.2 ± 1.1 s, Z = 0.001; P = 0.99; 4 Hz: 3.8 ± 0.3 s, Z = -2.197; P = 0.028; 8 Hz: 2.4 ± 0.3 s, Z = -2.366; P = 0.018; 16 Hz: 2.1 ± 0.3 s, Z = -2.366; P = 0.018; n = 7 neurons from five animals) compared to the lowest frequency tested (0.5 Hz: 6.5 ± 0.9 s), and values for decay time constant of the fluorescence responses of GACh2.0-expressing MEC stellate neurons to electrical stimulations consisting of a train of 20 pulses at higher frequency (1 Hz: 30.4 ± 3.1 s, Z = 0.169; P = 0.87; 2 Hz: 30.8 ± 2.0 s, Z = 0.338; P = 0.74; 4 Hz: 33.0 ± 2.1 s, Z = 0.338; P = 0.74; 8 Hz: 36.4 ± 6.1 s, Z = 1.363; P = 0.17; 16 Hz: 31.0 ± 2.4 s, Z = 0.169; P = 0.87; n = 7 neurons from nine animals) compared to the lowest frequency tested (0.5 Hz: 30.8 ± 5.7 s). **(i)** Fluorescence responses of GACh2.0-expressing MEC stellate neuron to electrical stimulations consisting of a train of up to 80 pulses at 2 Hz. **(j)** Values for the maximal responses of GACh2.0-expressing MEC stellate neurons to electrical stimulations consisting of a train of up to 80 pulses at 2 Hz (2 pulses: 0.70 ± 0.15%, Z = 1.960; P = 0.05; 5 pulses: 1.53 ± 0.38%, Z = 2.521; P = 0.012; 10 pulses: 2.22 ± 0.56%, Z = 2.521; P = 0.012; 20 pulses: 3.29 ± 0.95%, Z = 2.521; P = 0.012; 40 pulses: 4.07 ± 1.22%, Z = 2.366; P = 0.017; 80 pulse: 3.65 ± 1.30%, Z = 2.366; P = 0.017; n = 8 neurons from four animals) compared to single pulses (1 pulse: 0.50 ± 0.09%). **(k)** Values for 10–90% rise time of the maximal responses of GACh2.0-expressing MEC stellate neurons to electrical stimulations consisting of a train of up to 80 pulses at 2 Hz (two pulses: 1.8 ± 0.4 s, Z = 1.718; P = 0.08; 5 pulses: 2.0 ± 0.3 s, Z = 1.955; P = 0.05; 10 pulses: 3.3 ± 0.3 s, Z = 2.666; P = 0.008; 20 pulses: 5.0 ± 0.6 s, Z = 2.666; P = 0.008; 40 pulses: 6.5 ± 1.4 s, Z = 2.666; P = 0.008; n = 9 neurons from six animals) compared to single pulses (1 pulse: 1.3 ± 0.3 s), and decay time constant of the maximal responses of GACh2.0-expressing MEC stellate neurons to electrical stimulations consisting of a train of up to 80 pulses at 2 Hz (2 pulses: 32.2 ± 2.6 s, Z = -0.296; P = 0.77; 5 pulses: 33.9 ± 2.1 s, Z = 0.178; P = 0.86; 10 pulses: 32.8 ± 1.1 s, Z = -0.415; P = 0.68; 20 pulses: 32.7 ± 1.7 s, Z = -0.338; P = 0.75; 40 pulses: 31.8 ± 2.3 s, Z = -0.415; P = 0.68; n = 9 neurons from six animals) compared to single pulses (1 pulse: 32.9 ± 3.5 s). Note the stimulation pulse number-dependent increase in 10–90% rise time, but not in decay time constant. **(l)** A snapshot of another GACh2.0-expressing stellate cell. **(m)** Upper, snapshots of fluorescence responses of the GACh2.0-expressing neuron in **l** to a minimal L1 electrical stimulation. The fluorescence recording trace immediately below shows the average fluorescence response of the neuron. The lower fluorescence recording traces show ΔF/F₀ responses in the subcellular ROIs marked by colored squares (~1.5 μm × ~1.5 μm) in **l**. Note the largest ΔF/F₀ responses seen in two red ROIs (#9 and #1) suggestive of possible activation of multiple cholinergic fibers and/or release sites, and the slower rising times of smaller responses in other ROIs expected for diffused ACh. **(n)** Upper, plot of ΔF/F₀ responses in ROIs against the distance from the ROI with maximal ΔF/F₀. The data points (n = 67 from 6 neurons of six animals) were arbitrarily fitted to a single exponential decay function (pink line), resulting in an estimated volume spread length constant of ~9 μm. Lower, plot of ΔF/F₀ against F₀ indicates no correlation between ΔF/F₀ and F₀ (n = 67; two-sided Normality test, P = 0.06; two-sided Constant variance test, P = 0.80; r = 0.107; P = 0.39; two-sided Linear regression t test). The relative ΔF/F₀ responses, or the ΔF/F₀ responses normalized to the largest ΔF/F₀ responses in the same neurons, were used in analysis in **n**. Data are shown as mean ± s.e.m., where large black dots indicate mean response, error bars indicate s.e.m. Experiments in **b,d,f,i,l,m** were repeated independently for more than six animals with similar results. *P < 0.05 (Wilcoxon tests, two-sided).

We further examined the feasibility of optogenetic activation and optical imaging of cholinergic transmission simultaneously. We expressed DIO-oChIEF-tdTomato AAV in the basal forebrain of ChAT-Cre mice for 3 weeks, followed by Sindbis viral expression of GACh2.0 in MEC L2 stellate neurons for 18 h before preparing acute entorhinal cortical slices. We used single-photon LCD pulses (470 nm) to optogenetically stimulate oChIEF-expressing cholinergic fibers in MEC, and simultaneously used two-photon laser scanning (950 nm), which is insufficient to activate oChIEF-expressing fibers³⁶, to image fluorescence responses in GACh2.0-expressing stellate neurons in MEC (**Supplementary Fig. 20a**). Twenty 5-ms laser pulses (at 1 Hz) elicited consistent fluorescence responses in GACh2.0-expressing neurons, which were largely blocked by bath application of 20 μM PTAC (**Supplementary Fig. 20b,c**).

GACh sensors in non-neuronal tissues

ACh released from parasympathetic nerve terminals in the pancreas and adrenal is critical for insulin secretion³⁷ and regulation of stress and blood pressure³⁸, respectively. We made Sindbis viral expression of GACh2.0 in the mouse pancreas and adrenal *in vivo*, and imaged fluorescence responses of GACh2.0-expressing cells in acutely prepared pancreas and adrenal gland tissue slices (**Supplementary Figs. 21** and **22**). Single electrical stimulations of local parasympathetic cholinergic



fibers evoked evident fluorescence responses in GACH2.0-expressing pancreatic and adrenal cells (Supplementary Figs. 21b,c and 22b,c, and Supplementary Movies 6 and 7). Increasing the number of stimulation pulses delivered at 2 Hz progressively increased the amplitude of $\Delta F/F_0$ responses in pancreatic cells, while the responses plateaued with over ten pulses in adrenal cells (Supplementary Figs. 21d,e and 22d,e). Bath application of 20 μM PTAC blocked $\Delta F/F_0$ responses in GACH2.0-expressing pancreatic and adrenal cells (Supplementary Figs. 21f,g and 22f,g), confirming the cholinergic signals.

GACH sensors in transgenic *Drosophila* *in vivo*

Next, we tested whether GACH sensors detect cholinergic transmission in live *Drosophila*. We created UAS-GACH1.0 and UAS-GACH2.0

transgenic flies, and crossed them with a GH146-Gal4 driver line³⁹ to selectively express GACH1.0 and GACH2.0 in antennal lobe projection neurons, which receive abundant cholinergic inputs from olfactory receptor neurons⁴⁰. Two-photon imaging revealed that application of the odorant isoamyl acetate (IA) induced region-specific and dose-dependent $\Delta F/F_0$ responses in DM2 glomerulus, but not DA1 glomerulus^{41,42} (Fig. 5a–e). Application of the odor solvent, mineral oil alone did not evoke $\Delta F/F_0$ changes in transgenic flies (Fig. 5b,c). As expected, IA-evoked $\Delta F/F_0$ responses in GACH2.0 transgenic flies were about two-fold larger than those in GACH1.0 transgenic flies (Fig. 5d,e). Similarly, another odorant benzaldehyde also evoked region-specific and dose-dependent $\Delta F/F_0$ responses in the antennal lobe (Supplementary Fig. 23a–d). Moreover, IA elicited $\Delta F/F_0$ responses in the lateral horn,

a higher-order olfactory center of *Drosophila* as well (Supplementary Fig. 23e–g). Using the spectrum non-overlapping red Ca²⁺ indicator RGECO⁴³, we reexamined IA-induced responses in control GH146

> RGECO and GH146 > GACH1.0/2.0, RGECO transgenic flies. Application of IA induced the same Ca²⁺ transients in the DM2 glomerulus in control GH146 > RGECO, GH146 > GACH1.0, RGECO and

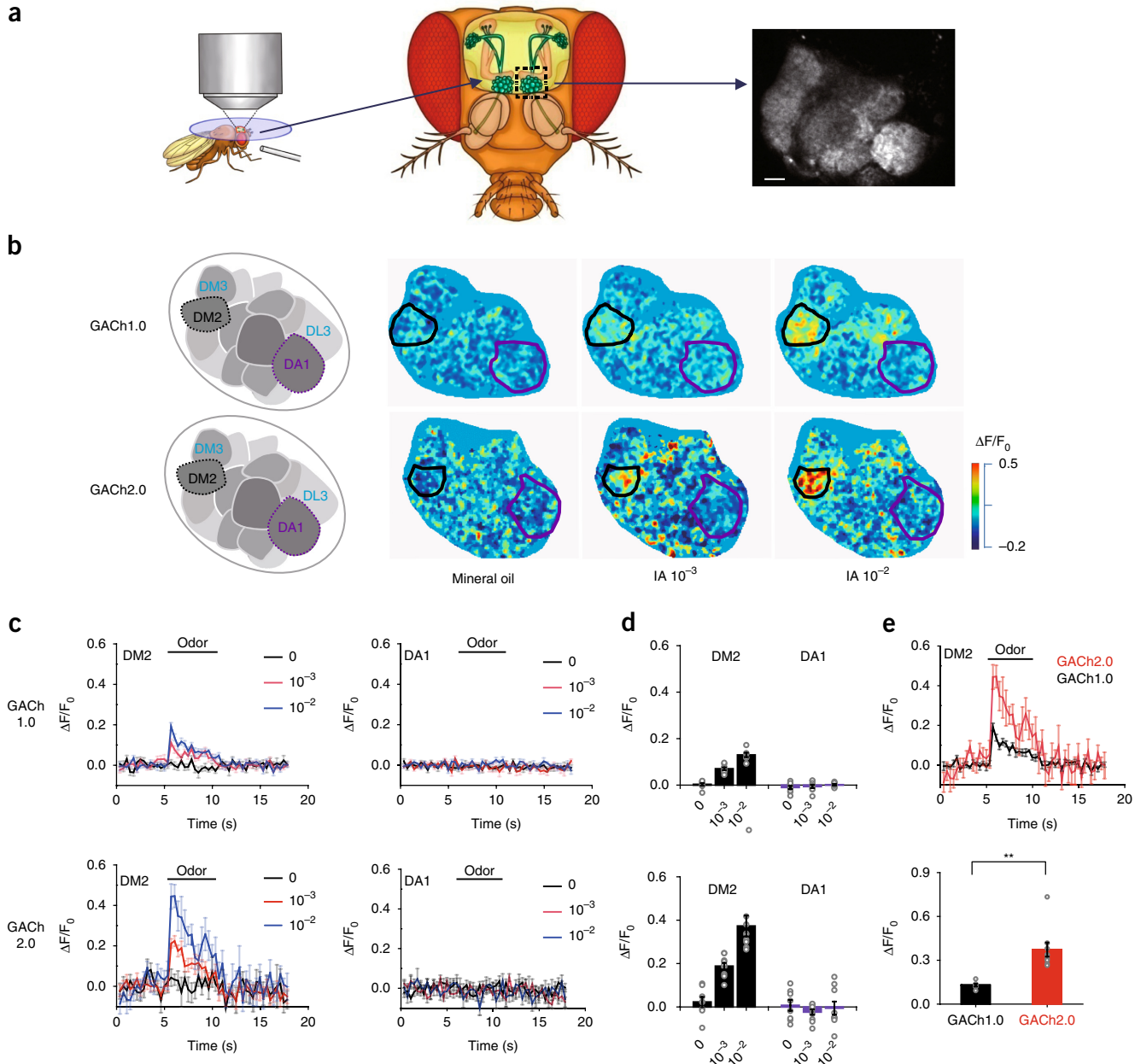


Figure 5 GACH sensors reveal dynamics of endogenous ACh release in *Drosophila*. **(a)** Schematic illustration of the two-photon imaging setup of the *Drosophila* olfactory system. Odor was delivered near the antenna (left), and GACH signals were measured in the antennal lobe area of GH146-Gal4:UAS-GACH flies (right). **(b)** Pseudocolor images of GACH-expressing antenna lobes show fluorescence responses to mineral oil and odor isoamyl acetate (IA). **(c)** Time courses of the IA-dependent responses in DM2 and DA1 glomeruli of GACH1.0- (upper plots) and GACH2.0- (lower plots) expressing antenna lobes. The traces were averaged from three trials in the same fly. **(d)** Values for the maximal $\Delta F/F_0$ in DM2 and DA1 glomeruli of GACH1.0-expressing antenna lobes (upper plot; DM2: $0.29 \pm 0.49\%$, $n = 9$ flies; DA1: $-1.01 \pm 0.68\%$, $n = 9$ flies, $U = 55$, $P = 0.22$ for mineral oil; DM2: $7.02 \pm 0.56\%$, $n = 9$ flies; DA1: $-0.61 \pm 0.80\%$, $n = 9$ flies, $U = 81$, $P = 4.12 \times 10^{-4}$ for 10^{-3} IA; DM2: $12.97 \pm 1.28\%$, $n = 7$ flies; DA1: $0.17 \pm 0.39\%$, $n = 7$ flies, $U = 49$, $P = 0.002$ for IA 10^{-2}) and GACH2.0-expressing antenna lobes (lower plot; DM2: $2.27 \pm 2.34\%$, $n = 8$ flies; DA1: $-0.73 \pm 1.41\%$, $n = 8$ flies, $U = 35$, $P = 0.80$ for mineral oil; DM2: $18.78 \pm 1.36\%$, $n = 10$ flies; DA1: $-2.37 \pm 1.06\%$, $n = 10$ flies, $U = 100$, $P = 1.83 \times 10^{-4}$ for 10^{-3} IA; DM2: $37.30 \pm 4.79\%$, $n = 9$ flies; DA1: $-0.55 \pm 2.68\%$, $n = 9$ flies, $U = 81$, $P = 4.12 \times 10^{-4}$ for 10^{-2} IA). **(e)** Upper, IA-evoked responses in DM2 glomerulus of GACH1.0 and GACH2.0 transgenic flies. Lower: values for the maximal $\Delta F/F_0$ in DM2 glomerulus of GACH1.0 and GACH2.0 transgenic flies (GACH1.0: $12.97 \pm 1.28\%$, $n = 7$ flies; GACH2.0: $37.30 \pm 4.79\%$, $n = 9$ flies; $U = 63$, $P = 0.001$). Data are shown as mean \pm s.e.m.; error bars indicate s.e.m. Experiments in **b** were repeated independently for more than seven flies with similar results. ** $P < 0.01$ (Mann–Whitney Rank Sum non-parametric tests, two-sided). All scale bars, 10 μ m.

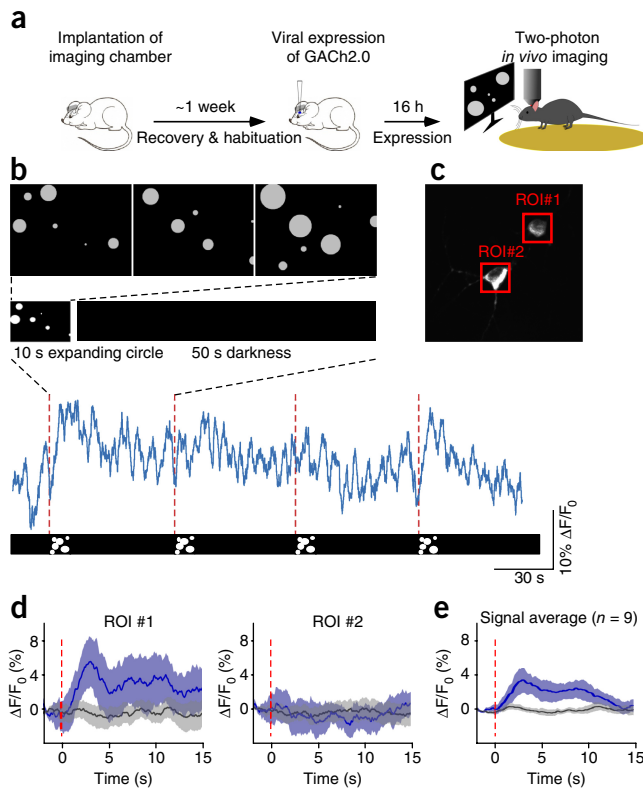


Figure 6 Attention-engaging visual stimuli evoke ACh release in behaving mice. (a) Schematic drawing outlines the design of *in vivo* imaging experiments. (b) Upper: schematic representation of the visual stimulus applied to head-fixed behaving mice. The visual stimulus consists of 10 s of expanding white circles appearing at random locations on the screen, followed by 50 s of darkness. Lower: four repetitions of single stimuli. (c) An imaged region ($100 \times 100 \mu\text{m}$, $120 \mu\text{m}$ deep) contains two GACH2.0-expressing neurons with the red squares indicating regions of interest (ROIs). (d) Mean fluorescence response traces from ROIs shown in b. The fluorescence response traces were divided into 10 s segments with every minute containing one 10-s trace corresponding to the period of visual stimulus and five 10-s traces corresponding to periods of darkness. The signal from the middle three dark segments (black line) was compared to the signal from the visual stimulus segments (blue line; 15 trials per region). Shaded bands around the solid blue trace show the 95% confidence interval obtained by bootstrap. Note that ROI #1, but not ROI #2, shows an increase in fluorescence responses to the visual stimulus. (e) Average fluorescence responses obtained during the period of visual stimulation compared to those during the period of darkness (visual: $3.37 \pm 2.26\%$; dark: $0.05 \pm 0.83\%$; $Z = -2.666$, $P = 0.008$; $n = 9$ neurons from eight animals). Note the same ACh signals observed after 1 d ($n = 5$ neurons from four animals), 2 d ($n = 2$ neurons from two animals), and 4–6 d ($n = 2$ neurons from two animals) *in vivo* Sindbis or rapid AAV viral expression, which suggest the suitability of GACH sensors for multiple-day imaging, and the analysis made from the pooled data. Data are shown as mean \pm s.e.m.; shaded bands indicate s.e.m. Wilcoxon tests performed in e, two-sided.

GH146 > GACH2.0, RGEKO transgenic flies (Supplementary Fig. 24), again ruling out the non-specific effect from GACH expression.

GACH sensors in mouse visual cortex *in vivo*

Finally, we tested the performance of GACH sensors by two-photon imaging in awake mouse L2/3 visual cortex⁴⁴ (Fig. 6a). We used a video monitor to deliver a visual stimulation consisting of 10-s images of expanding white-filled circles, which was designed

to elicit both attentional and visual responses ideal to trigger ACh release *in vivo*^{45–48}. The 10-s visual stimulation, but not the following 50-s darkness, reliably induced sustained fluorescence responses in some GACH-expressing neurons (Fig. 6b–d). However, some nearby expressing neurons exhibited no fluorescence responses to the same visual stimulation (Fig. 6b,c), suggesting a possible spatially specific visual-stimulation-evoked ACh release *in vivo* (Fig. 5 and Supplementary Fig. 16).

DISCUSSION

In this study, we have developed and validated a family of genetically encoded fluorescent ACh probes, GACH sensors. GACH sensors have the sensitivity, ligand specificity, SNR, kinetics, and photostability suitable for monitoring cholinergic signals in diverse tissue preparations *in vitro*, *ex vivo*, and *in vivo*. As with GCaMP3 (ref. 49) and iGluSnFR⁵⁰, the $\Delta F/F_0$ responses of GACH sensors in intact tissues are smaller than in cultured cells, presumably attributable to the higher tissue background/basal fluorescence. We also noted that GACH sensors have a weak coupling to downstream G-protein intracellular signaling in cultured cells, yet this coupling has no detectable effect on basic membrane properties, synaptic properties, and cholinergic transmission in rodent neurons *in vitro* and *in vivo*, as well as sensory input-evoked cholinergic responses in *Drosophila* *in vivo*.

Central cholinergic neurons exhibit multiple distinct action-potential firing patterns^{30,31,35}, yet the functional significance of these firing patterns remains elusive. Here we report that basal forebrain cholinergic neurons use low frequency 0.5–2 Hz tonic firing to generate large plateau-like postsynaptic ACh signals, and 8–12 Hz theta rhythmic phasic firing to elicit small transient postsynaptic ACh signals. A possible explanation is that the high-frequency activation of cholinergic fibers may be more effective in recruiting presynaptic auto-receptor inhibition mechanisms to suppress ACh release⁵¹, which yield more transient ACh signals. On the other hand, habenula neurons can fire high-frequency action potentials of up to 10–25 Hz³⁵. The firing triggers co-release of ACh with its primary neurotransmitter glutamate when a presynaptic GABA_BR-mediated potentiation mechanism is engaged. Although detailed aspects of cholinergic regulations remain to be worked out, our data are consistent with the view that presynaptic regulatory mechanisms may play key roles in governing release modes in central cholinergic transmission.

Another unresolved question concerns cholinergic volume transmission; whether ACh acts globally affecting a large number of neurons or mediates spatially restricted volume transmission remains a matter of debate^{1–3,13}. Directly visualizing the spread of released ACh in the hippocampus and MEC has allowed us to estimate the spread length constant of central cholinergic transmission, which ranges ~ 9 –15 μm . Because the minimal electrical stimulation may activate multiple ACh release sites, this value is likely to be overestimated. Nevertheless, the estimation provides the first suggestion that central cholinergic transmission may have single-cell or subcellular specificity. Since G-protein-coupled receptors may relay postsynaptic signaling in a highly spatially restricted manner⁵², it is tempting to speculate that intercellular cholinergic signal communication can achieve subcellular precision. Together, the findings of fine firing-frequency-controlled release and spatially restricted volume transmission advance our fundamental understanding of the regulation and precision of cholinergic signaling.

GACH sensors, which allow visualization of ACh signals in animal models *ex vivo* and *in vivo*, should advance our understanding of the pathogenesis of various diseases. For example, cholinergic signals are essential for high-level cognitive functions, including learning and

memory, and dysregulation of cholinergic transmission is linked with various neurological disorders, including Alzheimer's disease. Yet, the cholinergic hypothesis-based acetylcholinesterase inhibitor treatment, the only available therapy for Alzheimer's disease⁵³, has limited efficacy and is far from ideal^{34,54}. Further understanding of central cholinergic transmission in physiological and pathological conditions is central to development of effective therapeutic strategies for Alzheimer's disease and other neurological diseases. Moreover, defective cholinergic signals have been implicated in the pathophysiology and treatment of a number of other non-neurological diseases^{5–7}, including diabetes³⁷, cardiovascular diseases³⁸, inflammation⁵⁵, and tumorigenesis⁵⁶. We show here that GACh sensors are effective in monitoring cholinergic transmission in non-neuronal cells as well, including cells of the pancreas and adrenal, thus endorsing the use of this tool to unravel the cholinergic mechanisms underlying these pathological conditions.

METHODS

Methods, including statements of data availability and any associated accession codes and references, are available in the [online version of the paper](#).

Note: Any Supplementary Information and Source Data files are available in the online version of the paper.

ACKNOWLEDGMENTS

We thank L. Looger and colleagues for sharing their unpublished acetylcholine sensors that validated some of our results. We thank Y. Rao for generous sharing of two-photon microscopy. We are also grateful to L. Luo, S. Owen, Y. Rao, and L. Nevin for critical reading of the manuscript. We thank Z. Ye for the help in art designing. This work was supported by the National Basic Research Program of China (973 Program; grant 2015CB856402), The General Program of National Natural Science Foundation of China (project 31671118 and project 31371442), and the Junior Thousand Talents Program of China to Y.L. Additional support comes from NIH grants NS103558 (Y.L. and L.I.Z.), DC008983 (L.I.Z.), MH104227 and MH109475 (Y.Z.), MH109104 and NS022061 (L.W.R.), LH089717 (P.Q.B.), and NS053570, NS091452, NS094980, NS092548, and NS104670 (J.J.Z.). J.J.Z. is the Radboud Professor and Sir Yue-Kong Pao Chair Professor.

AUTHOR CONTRIBUTIONS

J.J.Z. and Y.L. conceived the project. M.J. did GACh screening and optimization as well as its validation in cultured neurons and IPN slices. Y.L., Y.S., Z.J.Z., and H.J. designed and performed the work on transgenic flies. M.J. and J.F. performed experiments related to calcium imaging, GPCR internalization, Tango assay, and FRET measurements. L.M. and L.Z. did *in vivo* imaging of GACh sensors in mouse visual cortex. M.L. supervised the imaging experiments on MHb-IPN brain slices. P.Z. and G.W. together carried out the other experiments with assistance and advice from S.W., J.C.L., N.A.G., L.W.L., J.L., Y.Z., D.A.T., L.W.R., P.Q.B., and J.J.Z. All authors contributed to data analysis. M.J., P.Z., G.W., J.J.Z., and Y.L. wrote the manuscript with input from other authors.

COMPETING INTERESTS

M.J. and Y.L. have filed patent applications whose value might be affected by this publication.

Reprints and permissions information is available online at <http://www.nature.com/reprints/index.html>. Publisher's note: Springer Nature remains neutral with regard to jurisdictional claims in published maps and institutional affiliations.

- Ballinger, E.C., Ananth, M., Talmage, D.A. & Role, L.W. Basal forebrain cholinergic circuits and signaling in cognition and cognitive decline. *Neuron* **91**, 1199–1218 (2016).
- Picciotto, M.R., Higley, M.J. & Mineur, Y.S. Acetylcholine as a neuromodulator: cholinergic signaling shapes nervous system function and behavior. *Neuron* **76**, 116–129 (2012).
- Dani, J.A. & Bertrand, D. Nicotinic acetylcholine receptors and nicotinic cholinergic mechanisms of the central nervous system. *Annu. Rev. Pharmacol. Toxicol.* **47**, 699–729 (2007).
- Dineley, K.T., Pandya, A.A. & Yakel, J.L. Nicotinic ACh receptors as therapeutic targets in CNS disorders. *Trends Pharmacol. Sci.* **36**, 96–108 (2015).
- Kruse, A.C. *et al.* Muscarinic acetylcholine receptors: novel opportunities for drug development. *Nat. Rev. Drug Discov.* **13**, 549–560 (2014).
- Soreq, H. Checks and balances on cholinergic signaling in brain and body function. *Trends Neurosci.* **38**, 448–458 (2015).
- Wessler, I. & Kirkpatrick, C.J. Acetylcholine beyond neurons: the non-neuronal cholinergic system in humans. *Br. J. Pharmacol.* **154**, 1558–1571 (2008).
- Ren, J. *et al.* Habenula "cholinergic" neurons co-release glutamate and acetylcholine and activate postsynaptic neurons via distinct transmission modes. *Neuron* **69**, 445–452 (2011).
- Williams, M.J. & Adinoff, B. The role of acetylcholine in cocaine addiction. *Neuropsychopharmacology* **33**, 1779–1797 (2008).
- Francis, P.T., Palmer, A.M., Snape, M. & Wilcock, G.K. The cholinergic hypothesis of Alzheimer's disease: a review of progress. *J. Neurol. Neurosurg. Psychiatry* **66**, 137–147 (1999).
- Vita, J.A. *et al.* Coronary vasomotor response to acetylcholine relates to risk factors for coronary artery disease. *Circulation* **81**, 491–498 (1989).
- Dang, N., Meng, X. & Song, H. Nicotinic acetylcholine receptors and cancer (Review). *Biomed. Rep.* **4**, 515–518 (2016).
- Sarter, M., Parikh, V. & Howe, W.M. Phasic acetylcholine release and the volume transmission hypothesis: time to move on. *Nat. Rev. Neurosci.* **10**, 383–390 (2009).
- Kodama, T., Lai, Y.Y. & Siegel, J.M. Enhancement of acetylcholine release during REM sleep in the caudomedial medulla as measured by *in vivo* microdialysis. *Brain Res.* **580**, 348–350 (1992).
- Schualo, O.N. *et al.* Carbon fibre-based microbiosensors for *in vivo* measurements of acetylcholine and choline. *Biosens. Bioelectron.* **21**, 87–94 (2005).
- Barnea, G. *et al.* The genetic design of signaling cascades to record receptor activation. *Proc. Natl. Acad. Sci. USA* **105**, 64–69 (2008).
- Ziegler, N., Bätz, J., Zabel, U., Lohse, M.J. & Hoffmann, C. FRET-based sensors for the human M1-, M3-, and M5-acetylcholine receptors. *Bioorg. Med. Chem.* **19**, 1048–1054 (2011).
- Markovic, D. *et al.* FRET-based detection of M1 muscarinic acetylcholine receptor activation by orthosteric and allosteric agonists. *PLoS One* **7**, e29946 (2012).
- Muller, A., Joseph, V., Slesinger, P.A. & Kleinfeld, D. Cell-based reporters reveal *in vivo* dynamics of dopamine and norepinephrine release in murine cortex. *Nat. Methods* **11**, 1245–1252 (2014).
- Nguyen, Q.T. *et al.* An *in vivo* biosensor for neurotransmitter release and *in situ* receptor activity. *Nat. Neurosci.* **13**, 127–132 (2010).
- Lin, M.Z. & Schnitzer, M.J. Genetically encoded indicators of neuronal activity. *Nat. Neurosci.* **19**, 1142–1153 (2016).
- Kruse, A.C. *et al.* Activation and allosteric modulation of a muscarinic acetylcholine receptor. *Nature* **504**, 101–106 (2013).
- Rasmussen, S.G. *et al.* Crystal structure of the human beta2 adrenergic G-protein-coupled receptor. *Nature* **450**, 383–387 (2007).
- Jakubík, J., Bacáková, L., El-Fakahany, E.E. & Tucek, S. Positive cooperativity of acetylcholine and other agonists with allosteric ligands on muscarinic acetylcholine receptors. *Mol. Pharmacol.* **52**, 172–179 (1997).
- Caulfield, M.P. & Birdsall, N.J. International Union of Pharmacology. XVII. Classification of muscarinic acetylcholine receptors. *Pharmacol. Rev.* **50**, 279–290 (1998).
- Papke, R.L. *et al.* The effects of subunit composition on the inhibition of nicotinic receptors by the amphiphatic blocker 2,2,6,6-tetramethylpiperidin-4-yl heptanoate. *Mol. Pharmacol.* **67**, 1977–1990 (2005).
- Shen, J. & Barnes, C.A. Age-related decrease in cholinergic synaptic transmission in three hippocampal subfields. *Neurobiol. Aging* **17**, 439–451 (1996).
- Eckenstein, F.P., Baughman, R.W. & Quinn, J. An anatomical study of cholinergic innervation in rat cerebral cortex. *Neuroscience* **25**, 457–474 (1988).
- Ray, S. *et al.* Grid-layout and theta-modulation of layer 2 pyramidal neurons in medial entorhinal cortex. *Science* **343**, 891–896 (2014).
- Simon, A.P., Poindessous-Jazat, F., Dutar, P., Epelbaum, J. & Bassant, M.H. Firing properties of anatomically identified neurons in the medial septum of anesthetized and unanesthetized restrained rats. *J. Neurosci.* **26**, 9038–9046 (2006).
- Dueque, A., Tepper, J.M., Detari, L., Ascoli, G.A. & Zaborszky, L. Morphological characterization of electrophysiologically and immunohistochemically identified basal forebrain cholinergic and neuropeptide Y-containing neurons. *Brain Struct. Funct.* **212**, 55–73 (2007).
- Bymaster, F.P. *et al.* Unexpected antipsychotic-like activity with the muscarinic receptor ligand (5R,6R)-6-(3-propylthio-1,2,5-thiadiazol-4-yl)-1-azabicyclo[3.2.1]octane. *Eur. J. Pharmacol.* **356**, 109–119 (1998).
- Zhang, J. *et al.* Presynaptic excitation via GABA_B receptors in habenula cholinergic neurons regulates fear memory expression. *Cell* **166**, 716–728 (2016).
- Zemek, F. *et al.* Outcomes of Alzheimer's disease therapy with acetylcholinesterase inhibitors and memantine. *Expert Opin. Drug Saf.* **13**, 759–774 (2014).
- Zhao, H. & Rusak, B. Circadian firing-rate rhythms and light responses of rat habenular nucleus neurons *in vivo* and *in vitro*. *Neuroscience* **132**, 519–528 (2005).
- Wang, G. *et al.* An optogenetics- and imaging-assisted simultaneous multiple patch-clamp recording system for decoding complex neural circuits. *Nat. Protoc.* **10**, 397–412 (2015).
- Satin, L.S. & Kinard, T.A. Neurotransmitters and their receptors in the islets of Langerhans of the pancreas: what messages do acetylcholine, glutamate, and GABA transmit? *Endocrine* **8**, 213–223 (1998).
- Ungar, A. & Phillips, J.H. Regulation of the adrenal medulla. *Physiol. Rev.* **63**, 787–843 (1983).

39. Stocker, R.F., Heimbeck, G., Gendre, N. & de Belle, J.S. Neuroblast ablation in *Drosophila* P[GAL4] lines reveals origins of olfactory interneurons. *J. Neurobiol.* **32**, 443–456 (1997).
40. Wilson, R.I. Early olfactory processing in *Drosophila*: mechanisms and principles. *Annu. Rev. Neurosci.* **36**, 217–241 (2013).
41. Ng, M. *et al.* Transmission of olfactory information between three populations of neurons in the antennal lobe of the fly. *Neuron* **36**, 463–474 (2002).
42. Wang, J.W., Wong, A.M., Flores, J., Vosshall, L.B. & Axel, R. Two-photon calcium imaging reveals an odor-evoked map of activity in the fly brain. *Cell* **112**, 271–282 (2003).
43. Zhao, Y. *et al.* An expanded palette of genetically encoded Ca^{2+} indicators. *Science* **333**, 1888–1891 (2011).
44. Ibrahim, L.A. *et al.* Cross-modality sharpening of visual cortical processing through layer-1-mediated inhibition and disinhibition. *Neuron* **89**, 1031–1045 (2016).
45. Letzkus, J.J. *et al.* A disinhibitory microcircuit for associative fear learning in the auditory cortex. *Nature* **480**, 331–335 (2011).
46. Niell, C.M. & Stryker, M.P. Modulation of visual responses by behavioral state in mouse visual cortex. *Neuron* **65**, 472–479 (2010).
47. Hasselmo, M.E. & Sarter, M. Modes and models of forebrain cholinergic neuromodulation of cognition. *Neuropsychopharmacology* **36**, 52–73 (2011).
48. Herrero, J.L. *et al.* Acetylcholine contributes through muscarinic receptors to attentional modulation in V1. *Nature* **454**, 1110–1114 (2008).
49. Tian, L. *et al.* Imaging neural activity in worms, flies and mice with improved GCaMP calcium indicators. *Nat. Methods* **6**, 875–881 (2009).
50. Marvin, J.S. *et al.* An optimized fluorescent probe for visualizing glutamate neurotransmission. *Nat. Methods* **10**, 162–170 (2013).
51. Alberts, P., Bartfai, T. & Stjärne, L. The effects of atropine on [^3H]acetylcholine secretion from guinea-pig myenteric plexus evoked electrically or by high potassium. *J. Physiol. (Lond.)* **329**, 93–112 (1982).
52. Sungkaworn, T. *et al.* Single-molecule imaging reveals receptor-G protein interactions at cell surface hot spots. *Nature* **550**, 543–547 (2017).
53. Mash, D.C., Flynn, D.D. & Potter, L.T. Loss of M_2 muscarine receptors in the cerebral cortex in Alzheimer's disease and experimental cholinergic denervation. *Science* **228**, 1115–1117 (1985).
54. Ashford, J.W. Treatment of Alzheimer's disease: the legacy of the cholinergic hypothesis, neuroplasticity, and future directions. *JAD* **47**, 149–156 (2015).
55. Tracey, K.J. Reflex control of immunity. *Nat. Rev. Immunol.* **9**, 418–428 (2009).
56. Magnon, C. *et al.* Autonomic nerve development contributes to prostate cancer progression. *Science* **341**, 1236361 (2013).

ONLINE METHODS

Animal preparation. Male and female Sprague–Dawley rats, and wild-type and ChAT-Cre transgenic C57BL/6 mice were used to prepare cultured neurons, cultured hippocampal slices, acute brain slices, acute pancreas, and adrenal slices in this study. Animals were maintained in the animal facilities at the Peking University, the National Institute of Biological Sciences, Beijing, China, University of Southern California, Stony Brook University, or the University of Virginia, and family or pair were housed in the temperature-controlled animal room with 12-h/12-h light/dark cycle. All procedures for animal surgery and maintenance were performed following protocols approved by the Animal Care & Use Committee of the Peking University, the National Institute of Biological Sciences, Beijing, China, University of Southern California, Stony Brook University or the University of Virginia and in accordance with US National Institutes of Health guidelines.

Preparations of cultured cells, cultured neurons and cultured slices.

HEK293T were cultured in DMEM (Gibco, MA) with 10% FBS (North TZ-Biotech Develop Co., Ltd, Beijing, China) at 37 °C, 5% CO₂, and passed to 12-mm glass coverslips in 24-well plates. Rat cortical neurons were prepared from postnatal 1-d-old (P1) Sprague–Dawley rats as previously described⁵⁷. Briefly, rat brains were dissected and digested by 0.25% Trypsin-EDTA (Gibco), and placed onto poly-d-lysine (Sigma-Aldrich, MO) coated coverslips with density of 0.5–1 × 10⁶ cells/ml.

Cultured slices were prepared from P6–7 rats or mice following our previous studies^{58,59}. In brief, the hippocampi were dissected out in ice-cold HEPES-buffered Hanks' solution (pH 7.35) under sterile conditions, sectioned into 400 µm slices on a tissue chopper, and explanted onto a Millicell-CM membrane (0.4-µm pore size; Millipore, MA). The membranes were then placed in 750 µl of MEM culture medium, contained (in mM): HEPES 30, heat-inactivated horse serum 20%, glutamine 1.4, D-glucose 16.25, NaHCO₃ 5, CaCl₂ 1, MgSO₄ 2, insulin 1 mg/ml, ascorbic acid 0.012% at pH 7.28 and osmolarity 320. Cultured slices were maintained at 35 °C, in a humidified incubator (ambient air enriched with 5% CO₂).

Preparations of acute tissue slices. Acute thalamic, barrel cortical, entorhinal cortical, hippocampal, and MHb-fr-IPN brain slices, pancreas, and adrenal tissues slices were prepared from P25–60 animals deeply anesthetized by xylazine-ketamine or pentobarbital (100 mg/kg) as described in our previous reports^{59,60}. The animals were decapitated and the brain block containing the thalamus, barrel cortex, MEC and/or hippocampus, the pancreas, or the adrenal was quickly removed and placed into cold (0–4 °C) oxygenated physiological solution containing (in mM): 125 NaCl, 2.5 KCl, 1.25 NaH₂PO₄, 25 NaHCO₃, 1 MgCl₂, 25 dextrose, and 2 CaCl₂, pH 7.4. The brain blocks were directly sectioned into 400-µm-thick brain slices using a DSK microslicer (Ted Pella Inc.), while the pancreas and adrenal were first embedded in low-melting-temperature agar (2.5% in BBS) and then sectioned into 400-µm-thick tissue slices⁶¹. For the MHb-fr-IPN slice preparation, the brains were first blocked at ~45° angle from the horizontal plane and then sectioned into 250-µm-thick slices by VT1200 vibratome (Leica, Germany). The tissue slices were kept at 37.0 ± 0.5 °C in oxygenated physiological solution for ~0.5–1 h before imaging. During the recording and/or imaging the slices were submerged in a chamber and stabilized with a fine nylon net attached to a platinum ring. The recording chamber was perfused with oxygenated physiological solution. The half-time for the bath solution exchange was ~6 s, and the temperature of the bath solution was maintained at 34.0 ± 0.5 °C. All antagonists were bath-applied. Distinct cell types, including L2 stellate neurons and L1 interneurons in MEC⁶², L5 pyramidal neurons in the barrel cortex of mice^{59,63,64}, GABAergic thalamic reticular neurons and glutamatergic thalamocortical neurons in the ventral basal nucleus of rats^{59,65}, could be easily identified under transmitted light illumination based on their locations and somatodendritic morphology as characterized in the previous reports.

Molecular biology. Molecular cloning was typically carried out using the Gibson assembly⁶⁶ with ~30 overlapping base primers and the Phusion DNA polymerase (New England BioLabs, MA), and verified by Sanger sequencing using an in-house facility (sequencing platform in the School of Life Sciences of the Peking University). The chimeric GACh constructs were generated

by subcloning full-length human GPCR cDNAs (hORFeome database 8.1, the Dana-Farber Cancer Institute Center for Cancer Systems Biology) into the pDisplay vector (Invitrogen, MA), with an IgK leader sequence inserted before the coding region. The site-directed mutagenesis of the sequences of the two- and five-amino acid linkers in the N and C termini of cpGFP was made using primers containing various lengths of tri-nucleotides NNB (20 possible amino acids, Sangon Biotech, Shanghai, China). The applicable GACh sensors were then subcloned into the Sindbis viral vector, the lentiviral vector, or the AAV package vector under the human synapsin promoter to ensure the neuronal expression. To create the transgenic *Drosophila*, fragments of GACh sensors including the IgK leader sequence were cloned into the pUAST vector, and subsequently injected into *Drosophila* embryo following a standard protocol (Fungene Biotechnology, Beijing). To report the receptor endocytosis, super-ecliptic pHluorin⁶⁷ was cloned to the N terminus of M₃R, with a three amino acid linker (GGA) to ensure correct protein folding and trafficking.

Expression of GACh sensors and other recombinant proteins. HEK293T cells were typically transfected using the polyethylenimine (PE) method (with a typical ratio of 1 µg DNA to 4 µg PEI), media replaced 4–6 h later, and cells imaged 24 h later. Cultured neurons were transfected after 7–9 d *in vitro* using the calcium phosphate transfection method and experiments were performed 48 h after transfection. Neurons in hippocampal cultured slices were infected after 8–18 d *in vitro* with lentivirus or Sindbis virus, and then incubated on culture media and 5% CO₂ before experiments. For *in vivo* expression, P28–84 animals were initially anesthetized by an intraperitoneal injection of 2,2,2-Tribromoethanol (Avetin, 500 mg/kg) or ketamine and xylazine (10 and 2 mg/kg, respectively), and then placed in a stereotaxic frame. In some of the animals, AAV of GACh sensors (with a titer of >10¹²/ml) was injected into IPN with a microsyringe pump (Nanoliter 2000 Injector, WPI) using the coordinates (AP: -3.13 mm from Bregma; DV: -4.95 mm; ML: 1.33 mm with 15° angle toward the midline), or into the dentate gyrus of hippocampus (AP: -1.80 mm from Bregma; DV: -1.80 mm; ML: 0.80 mm). In other animals, a glass pipette was used to penetrate into the thalamic ventrobasal nucleus, thalamic reticular nucleus, the barrel cortex and MEC according to stereotaxic coordinates, or the dissected pancreas and adrenal, to deliver ~50 nl of viral solution by pressure injection to infect neurons, or pancreas and adrenal cells with GACh sensors. In ChAT-Cre transgenic mice, AAV of DIO-oChIEF-tdTomato was first injected into basal forebrain according to the previously described coordinates⁶⁸, and 3 weeks later, Sindbis virus of GACh sensors was injected into MEC for ~18 h before preparing acute brain slices for experiments.

Electrophysiology. Simultaneous dual whole-cell recordings were obtained from two nearby infected and non-infected hippocampal CA1 pyramidal neurons under visual guidance using fluorescence and transmitted light illumination^{59,60}. The patch recording pipettes (4–7 M) were filled with intracellular solution containing 115 mM cesium methanesulfonate, 20 mM CsCl, 10 mM HEPES, 2.5 mM MgCl₂, 4 mM Na₂ATP, 0.4 mM Na₃GTP, 10 mM sodium phosphocreatine, 0.6 mM EGTA, and 0.1 mM spermine and 0.5% biocytin (pH 7.25) for voltage-clamp recordings, or containing 120 mM potassium gluconate, 4 mM KCl, 10 mM HEPES, 4 mM MgATP, 0.3 mM Na₃GTP, 10 mM sodium phosphocreatine, and 0.5% biocytin (pH 7.25) for current-clamp recordings. Bath solution (29 ± 1.5 °C) contained (in mM): NaCl 119, KCl 2.5, CaCl₂ 4, MgCl₂ 4, NaHCO₃ 26, NaH₂PO₄ 1, glucose 11, picrotoxin (PTX) 0.1, bicuculline 0.01, and 2-chloroadenosine 0.002, at pH 7.4 and gassed with 5% CO₂/95% O₂. PTX was excluded when GABA responses were examined. Whole-cell recordings were made with up to two Axoclamp 2B or Axopatch-200B patch clamp amplifiers (Molecular Devices, Sunnyvale, CA). Junction potentials were not corrected. Synaptic responses were evoked by bipolar electrodes with single-voltage pulses (200 µs, up to 20 V). Synaptic AMPA and NMDA responses at -60 mV and +40 mV or GABA responses at 0 mV were averaged over 90 trials. To minimize the effect from AMPA responses, the peak NMDA responses at +40 mV were measured after digital subtraction of estimated AMPA responses at +40 mV. Cholinergic fibers in tissue slices were stimulated with a bipolar electrode placed ~50–200 µm from imaged cells with single or a train of voltage pulses (500 µs, up to 50 V) to evoke ACh release.

Fluorescence imaging of cultured cells and neurons. In some experiments, the fluorescence signals of HEK293T cells transfected with the muscarinic receptor-based chimeric constructs were measured with a TECAN Safire2 fluorescence plate reader (TECAN, Männedorf, Switzerland; excitation, 480 nm; emission, 520 nm). During the measurement, the culture media was replaced with 100 μ l Tyrode solution containing ACh at varied concentrations from 0–100 μ M. The $\Delta F/F_0$ of each construct was obtained by averaging the ACh-induced fluorescence responses of transfected wells after digitally subtracting that of neighboring control non-transfected wells.

In other culture cell experiments, HEK293T cells and cultured neurons were imaged by an inverted Nikon Ti-E A1 confocal microscope with a 40 \times /1.35 NA oil objective (Nikon, Tokyo, Japan). Cells were perfused with standard extracellular Tyrode solution containing (in mM): 150 NaCl, 4 KCl, 2 MgCl₂, 2 CaCl₂, 10 HEPES and 10 Glucose, with pH of 7.4, in an imaging chamber during imaging. Agonist acetylcholine (Solarbio, Beijing, China), tiotropium bromide (Dexinjia Bio & Tech Co., Ltd, Jinan, China), and AF-DX 384 (Sigma-Aldrich) were delivered with a custom-made perfusion system and/or bath applied. The chamber was washed with Tyrode solution between applications and cleaned with 75% ethanol between experiments.

Fluorescence imaging of cells in cultured and acute slice preparations. Wide-field epifluorescence imaging was performed using Hamamatsu ORCA FLASH4.0 camera (Hamamatsu Photonics, Japan), and GACh-expressing cells in cultured hippocampal slices and acutely prepared brain slices are excited by a 460-nm ultrahigh-power low-noise LED (Prizmatix, Givat-Shmuel, Israel). The frame rate of FLASH4.0 camera was set to 10 Hz. To synchronize image capture with drug perfusion, electrical stimulation, and/or electrophysiological recording, the camera was set to external trigger mode and triggered by a custom-written IGOR Pro 6 program (WaveMetrics, Lake Oswego, OR). Agonists or antagonists, including acetylcholine and atropine (Sigma-Aldrich), and nicotine, oxotremorine M, PTAC and TMPH (Tocris Bioscience, Bristol, UK), were either bath-applied or puff-applied with a glass pipette (~1 μ m in tip diameter) positioned ~150 μ m above the imaged neurons using 500-ms 30-kPa pressure pulses.

Two-photon imaging was performed using a custom-built microscope or an Olympus FV1000 microscope (for IPN experiments; Olympus, Japan). The parameters of frame scan were typically set at a size of 200 \times 200 pixels and a speed of 1 frame/s. For all optical experiments, the actual two-photon scanning time was set at ~700 ms/frame, and 20 10-ms 470-nm blue M470F LED (Thorlabs, NJ) light pulses were synchronously delivered at 1 Hz during the ~300-ms frame scanning break periods to activate oChIEF-tdTomato expressing cholinergic fibers without interfering two-photon imaging. The blue light of the LED was fiber-coupled to an Ø200 μ m fiber optic cannula positioned ~250 μ m away from imaged neurons. The light power out of the cannula was set at 2 mW. The fluorescence of GACh2.0 was excited by a femtosecond Ti:Sapphire laser (Chameleon Ultra II, Coherent) at a wavelength of 950 nm. Changes in fluorescence were quantified as increases in fluorescence from baseline divided by resting fluorescence ($\Delta F/F_0$) and averaged for ~10 trials. To quantify surface expression of GACh sensors, lentiviral expression of GACh1.0, GACh1.5, or GACh2.0 was made in the CA1 region of organotypic hippocampal cultured slices. About ~1–2 weeks after expression, GACh-expressing CA1 pyramidal neurons were patch-clamp recorded and loaded with 25 μ M Alexa Fluor 594 (Life Technologies) for ~10 min, and two-photon images were then taken at different compartments along the apical dendrites. The multiple patch-clamp recordings, optogenetics, epifluorescence, and two-photon imaging were typically operated by a single custom-written IGOR Pro 6 program (WaveMetrics, Lake Oswego, OR). To image the high KCl-induced calcium signals, 20 μ M Cal590F (AAT Bioquest Inc., Sunnyvale, CA) was bath-loaded into hippocampal cells in acute slices and subsequently washed with ACSF for 30 min before imaging. Cal590 dye was excited with a two-photon laser at 950 nm, and 90 mM KCl was perfused to stimulate calcium signals.

Immunocytochemistry. Mice infected with GACh sensors were deeply anesthetized with pentobarbital (400 mg/kg; i.p.), and transcardially perfused first with cold normal saline and then 4% paraformaldehyde in 0.1 M PBS. Brain blocks were post-fixed for ≥4 h, cryoprotected in 30% sucrose for ≥24 h,

then embedded in tissue freezing medium and sectioned into 50- μ m-thick coronal sections with a freezing Leica CM 1900 microtome (Leica, Germany). To label cholinergic terminals from MHb- and GACh-expressing neurons in IPN, tissue sections were rinsed and immunoreacted with goat ChAT antibody (1:500, Millipore, #ab144p) and rabbit GFP antibody (1:500, Abcam, #ab6556), and then labeled with goat anti-rabbit second antibody conjugated Alexa 488 and donkey anti-goat second antibody conjugated Alexa 555 after extensive washing. The immunolabeled tissue sections were imaged with a confocal microscope.

To recover the morphology of recorded neurons, the slices were fixed by immersion in 3% acrolein/4% paraformaldehyde in 0.1 M PBS at 4 °C for 24 h after *in vitro* patch-clamp recordings with internal solution containing additional 1% biocytin, and then processed with the avidin-biotin-peroxidase method to reveal cell morphology. The morphologically recovered cells were examined and reconstructed with the aid of a microscope equipped with a computerized reconstruction system Neurolucida (MicroBrightField, Colchester, VT).

Fluorescence imaging of transgenic *Drosophila*. Transgenic *Drosophila* lines with strong GACh expression levels and robust odor responses were chosen after crossing UAS-GACh1.0 and UAS-GACh2.0 transgenic flies with a GH146-Gal4 driver line. They were reared at room temperature for 8~12 d on standard medium after eclosion before experiments. For imaging experiments, live flies were mounted and prepared as in our previous study⁶⁹. Briefly, animals were mounted to a small dish, with their rectangular patch of cuticle between the eyes, excessive fat bodies and air sacs surrounding the antennal lobe removed, and the pair of muscles underneath the proboscis cut to reduce the brain movement. Isoamyl acetate (Sigma-Aldrich; Cat# 306967) and benzaldehyde (Sinopharm Chemical Reagent Co., Ltd., Shanghai, China, Cat# 30017018) were initially diluted by 100-fold or 1000-fold (vol/vol) in mineral oil (Sigma-Aldrich; Cat# 69794) and then placed in a glass bottle (100 μ l in 900 μ l mineral oil), delivered at 200 ml/min, and mixed with purified air (1000 ml/min). The mixed air stream was presented to flies through a 1-cm-wide opening Teflon tube placed ~1 cm from their antennas, and controlled by Teflon solenoid valves and synchronized with the image acquisition system by Arduino boards. Imaging was made using a commercial Olympus BX61WI two-photon microscope with a 25 \times /NA: 1.05 water-immersion objective and a mode-locked Ti:Sapphileaser (Mai tai) tuned to 950 nm. The Glomeruli were identified according to the previous established antennal lobe map⁷⁰.

Fluorescence imaging of behaving mice. Mice were initially anesthetized to remove the head skin to attach a metal recording chamber, followed by a 3–5-day recovery and another 2–5-day head-fixation habituation. The animals were then anesthetized again to open the skull above the primary visual cortex (centered ~2.5 lateral, ~1.5 mm anterior from lambda) to pressure inject ~100 nl of Sindbis virus of GACh2.0 or AAV viruses of hsyn-tTA and TRE-GACh2.0 (with a 1:1 mix ratio; a speeded AAV expression approach⁷¹). The craniotomy was completed by fitting a cranial window made with a 3-mm circular or a 2 \times 2 mm square #2 coverslip. About 16 h after the surgery, the animals were head-fixed on a circular treadmill and imaged using a custom-built 2-photon system powered with an InSight DS+ laser (Spectra Physics) and operated with ScanImage 5.1 software⁷². Images were acquired from individual cells (or small groups of cells when possible) continuously at either 30 Hz (512 \times 512 pixels) or 60 Hz (256 \times 256 pixels). The mouse was shown a stimulus consisting of 50 s of darkness followed by 10 s of expanding white circles appearing at random positions on the screen. All data analysis was done in Matlab (Mathworks). Automatic image alignment was validated by manual inspection. ROIs were manually drawn over the cell bodies and raw fluorescent traces were extracted. Fluorescent traces were filtered by a 2 s moving average window to reduce fluctuations, and divided into 10 s segments corresponding to either periods of darkness or periods of visual stimulation, and the maximum $\Delta F/F_0$ was compared for periods with or without stimulation.

Statistical analysis. Statistical results were reported as mean \pm s.e.m. The signal-to-noise ratio (SNR) was calculated as the peak response dividing the standard error of baseline fluorescence. Animals were randomly assigned into control or experimental groups and investigators were blinded to experiment treatments.

Given the negative correlation between the variation and square root of sample number, n , the group sample size was typically set to be ~10–25 to optimize the power of statistical tests and efficiency. Statistical significance of the means ($P < 0.05$; two sides) were determined using Wilcoxon and Mann–Whitney Rank Sum non-parametric tests for paired and unpaired samples, respectively. Statistical significances of the linear relationships of two data groups were determined using linear regression t tests provided the normality and constant variance tests passed.

Life Sciences Reporting Summary. Further information on experimental design is available in the Nature Research Reporting Summary linked to this article.

Data availability. The plasmid pDisplay-GACh2.0 (#106073) has been deposited to the Addgene database (deposit #74965).

57. Zhang, Q., Li, Y. & Tsien, R.W. The dynamic control of kiss-and-run and vesicular reuse probed with single nanoparticles. *Science* **323**, 1448–1453 (2009).
58. Qin, Y. *et al.* State-dependent Ras signaling and AMPA receptor trafficking. *Genes Dev.* **19**, 2000–2015 (2005).
59. Wang, G. *et al.* Ca₃.2 calcium channels control NMDA receptor-mediated transmission: a new mechanism for absence epilepsy. *Genes Dev.* **29**, 1535–1551 (2015).
60. Lim, C.S. *et al.* BRAF signaling principles unveiled by large-scale human mutation analysis with a rapid lentivirus-based gene replacement method. *Genes Dev.* **31**, 537–552 (2017).
61. Hu, C., Rusin, C.G., Tan, Z., Guagliardo, N.A. & Barrett, P.Q. Zona glomerulosa cells of the mouse adrenal cortex are intrinsic electrical oscillators. *J. Clin. Invest.* **122**, 2046–2053 (2012).
62. Canto, C.B. & Witter, M.P. Cellular properties of principal neurons in the rat entorhinal cortex. II. The medial entorhinal cortex. *Hippocampus* **22**, 1277–1299 (2012).
63. Zhu, J.J. Maturation of layer 5 neocortical pyramidal neurons: amplifying salient layer 1 and layer 4 inputs by Ca²⁺ action potentials in adult rat tuft dendrites. *J. Physiol. (Lond.)* **526**, 571–587 (2000).
64. Zhu, J.J. Activity level-dependent synapse-specific AMPA receptor trafficking regulates transmission kinetics. *J. Neurosci.* **29**, 6320–6335 (2009).
65. Zhu, J.J. & Uhlrich, D.J. Nicotinic receptor-mediated responses in relay cells and interneurons in the rat lateral geniculate nucleus. *Neuroscience* **80**, 191–202 (1997).
66. Gibson, D.G. *et al.* Enzymatic assembly of DNA molecules up to several hundred kilobases. *Nat. Methods* **6**, 343–345 (2009).
67. Miesenböck, G., De Angelis, D.A. & Rothman, J.E. Visualizing secretion and synaptic transmission with pH-sensitive green fluorescent proteins. *Nature* **394**, 192–195 (1998).
68. Jiang, L. *et al.* Cholinergic signaling controls conditioned fear behaviors and enhances plasticity of cortical-amygdala circuits. *Neuron* **90**, 1057–1070 (2016).
69. Liang, L. *et al.* GABAergic projection neurons route selective olfactory inputs to specific higher-order neurons. *Neuron* **79**, 917–931 (2013).
70. Laiusse, P.P. *et al.* Three-dimensional reconstruction of the antennal lobe in *Drosophila melanogaster*. *J. Comp. Neurol.* **405**, 543–552 (1999).
71. Liu, B., Wang, S., Brenner, M., Paton, J.F. & Kasparyan, S. Enhancement of cell-specific transgene expression from a Tet-Off regulatory system using a transcriptional amplification strategy in the rat brain. *J. Gene Med.* **10**, 583–592 (2008).
72. Pologruto, T.A., Sabatini, B.L. & Svoboda, K. ScanImage: flexible software for operating laser scanning microscopes. *Biomed. Eng. Online* **9**, 1–9 (2003).

Life Sciences Reporting Summary

Nature Research wishes to improve the reproducibility of the work that we publish. This form is intended for publication with all accepted life science papers and provides structure for consistency and transparency in reporting. Every life science submission will use this form; some list items might not apply to an individual manuscript, but all fields must be completed for clarity.

For further information on the points included in this form, see [Reporting Life Sciences Research](#). For further information on Nature Research policies, including our [data availability policy](#), see [Authors & Referees](#) and the [Editorial Policy Checklist](#).

► Experimental design

1. Sample size

Describe how sample size was determined.

No statistical methods were used to pre-determine sample sizes, but given the negative correlation between the variation and square root of sample number, n , the group sample size was typically set to be $\sim 10-25$ to optimize the power of statistical tests and efficiency.

2. Data exclusions

Describe any data exclusions.

No data was excluded from the analysis.

3. Replication

Describe whether the experimental findings were reliably reproduced.

Each data in this manuscript is reliably reproduced. The replication number of each data is indicated in the legend of corresponding figures.

4. Randomization

Describe how samples/organisms/participants were allocated into experimental groups.

Animals or cells were randomly assigned into control or experimental groups.

5. Blinding

Describe whether the investigators were blinded to group allocation during data collection and/or analysis.

No blinding was carried out in sensor development and characterizations in cultured cells, which refer to data in Fig. 1-2. For slice and in vivo experiments in Fig. 3-8, investigators were blinded to the group allocation during the experiment.

Note: all studies involving animals and/or human research participants must disclose whether blinding and randomization were used.

6. Statistical parameters

For all figures and tables that use statistical methods, confirm that the following items are present in relevant figure legends (or in the Methods section if additional space is needed).

n/a Confirmed

- The exact sample size (n) for each experimental group/condition, given as a discrete number and unit of measurement (animals, litters, cultures, etc.)
- A description of how samples were collected, noting whether measurements were taken from distinct samples or whether the same sample was measured repeatedly
- A statement indicating how many times each experiment was replicated
- The statistical test(s) used and whether they are one- or two-sided (note: only common tests should be described solely by name; more complex techniques should be described in the Methods section)
- A description of any assumptions or corrections, such as an adjustment for multiple comparisons
- The test results (e.g. P values) given as exact values whenever possible and with confidence intervals noted
- A clear description of statistics including central tendency (e.g. median, mean) and variation (e.g. standard deviation, interquartile range)
- Clearly defined error bars

See the web collection on [statistics for biologists](#) for further resources and guidance.

► Software

Policy information about [availability of computer code](#)

7. Software

Describe the software used to analyze the data in this study.

The imaging data was process by imageJ(NIH), and data was process by matlab (Mathwork) and plotted in Origin(OriginLab).

For manuscripts utilizing custom algorithms or software that are central to the paper but not yet described in the published literature, software must be made available to editors and reviewers upon request. We strongly encourage code deposition in a community repository (e.g. GitHub). [Nature Methods guidance for providing algorithms and software for publication](#) provides further information on this topic.

► Materials and reagents

Policy information about [availability of materials](#)

8. Materials availability

Indicate whether there are restrictions on availability of unique materials or if these materials are only available for distribution by a for-profit company.

9. Antibodies

Describe the antibodies used and how they were validated for use in the system under study (i.e. assay and species).

The plasmid pDisplay-GACh2.0 (#106073) have been deposited to Addgene database (deposit #74965).

Goat anti-choline acetyltransferase(ChAT) antibody(1:500, Millipore, #ab144p, Lot:#2971003, also see Juen Zhang, et al, Cell, 2016, Pubmed 27426949); Rabbit anti-GFP antibody(1:500, Abcam, #ab6556, Lot:#GR277888-1, also see Wein MN, et al, Nat Commun, 2016, Pubmed 27759007); Secondary antibody goat anti rabbit iFluor-488 (1:500, AAT-Bio, #16687, Lot:#1060423) and secondary antibody Cy3-conjugated donkey anti goat (1:500, Jackson ImmunoResearch, #705-165-147, Lot:#107582) were used in immunostaining of MHB-IPN slices.

10. Eukaryotic cell lines

a. State the source of each eukaryotic cell line used.

The cell lines used in this paper is HEK293T cell line, which is listed in the list of ICLAC. It was passaged from a neighbor lab, which was originally bought from ATCC(catalog: ATCC® CRL-3216™)

b. Describe the method of cell line authentication used.

We have authenticated this cell line based on the morphology under microscope and the analysis of the growth curve.

c. Report whether the cell lines were tested for mycoplasma contamination.

No. We haven't tested the cell line for mycoplasma contamination. However, as these cells are used for sensor expression and screening, it will not affect our conclusion.

d. If any of the cell lines used are listed in the database of commonly misidentified cell lines maintained by ICLAC, provide a scientific rationale for their use.

No commonly misidentified cell lines were used.

► Animals and human research participants

Policy information about [studies involving animals](#); when reporting animal research, follow the [ARRIVE guidelines](#)

11. Description of research animals

Provide details on animals and/or animal-derived materials used in the study.

New borne male and female Sprague Dawley rats (P1) were used in Fig. 2f-j and Fig. S8 for primary cortical neuron dissection and culture. Male and Female wild type C57BL/6 mice with the age of P25-60 were used in Fig. 3-6, Fig. 8, Fig. S10-S19 and Fig. S21 for preparing acute brain, pancreas and adrenal slices and in vivo two photon imaging experiments. Male and female Sprague Dawley rats with the age of P25-60 were used in Fig. S14. Male and female ChAT-cre transgenic C57BL/6 mice with the age of P25-60 were used in Fig. S20 for acute brain slice preparation. Transgenic Drosophila which are 8-12 days after eclosion were used in Fig. 7,22,23 for live fly imaging experiments.

Policy information about [studies involving human research participants](#)

12. Description of human research participants

Describe the covariate-relevant population characteristics of the human research participants.

The study did not involve human research participants.